HHS Public Access

Author manuscript

Cell Rep. Author manuscript; available in PMC 2022 June 06.

Published in final edited form as:

Cell Rep. 2021 February 02; 34(5): 108723. doi:10.1016/j.celrep.2021.108723.

An IDH1-vitamin C crosstalk drives human erythroid development by inhibiting pro-oxidant mitochondrial metabolism

Pedro Gonzalez-Menendez[1,2,10,*], **Manuela Romano**[1,2,10], **Hongxia Yan**[1,3], **Ruhi Deshmukh**[4], **Julien Papoin**[5], **Leal Oburoglu**[1,2], **Marie Daumur**[1,2], **Anne-Sophie Dumé**[1,2], **Ira Phadke**[1,2,6], **Cédric Mongellaz**[1,2], **Xiaoli Qu**[3], **Phuong-Nhi Bories**[7], **Michaela Fontenay**[2,7], **Xiuli An**[3], **Valérie Dardalhon**[1,2], **Marc Sitbon**[1,2], **Valérie S. Zimmermann**[1,2], **Patrick G. Gallagher**[8], **Saverio Tardito**[4,9], **Lionel Blanc**[5], **Narla Mohandas**[3], **Naomi Taylor**[1,2,6,11,*], **Sandrina Kinet**[1,2,*]

[1]Institut de Génétique Moléculaire de Montpellier, Univ. Montpellier, CNRS, Montpellier, France

[2]Laboratory of Excellence GR-Ex, Paris 75015, France

[3]New York Blood Center, New York, NY, USA

[4]Cancer Research UK Beatson Institute, Glasgow G61 1BD, UK

[5]The Feinstein Institute for Medical Research, Manhasset, NY, USA

[6]Pediatric Oncology Branch, NCI, CCR, NIH, Bethesda, MD, USA

[7]Service d'Hématologie Biologique, Assistance Publique-Hôpitaux de Paris, Institut Cochin, Paris, France

[8]Departments of Pediatrics and Genetics, Yale University School of Medicine, New Haven, CT, USA

[9]Institute of Cancer Sciences, University of Glasgow, Glasgow G61 1QH, UK

[10]These authors contributed equally

[11]Lead contact

SUMMARY

The metabolic changes controlling the stepwise differentiation of hematopoietic stem and progenitor cells (HSPCs) to mature erythrocytes are poorly understood. Here, we show that HSPC development to an erythroid-committed proerythroblast results in augmented glutaminolysis, generating alpha-ketoglutarate (αKG) and driving mitochondrial oxidative phosphorylation (OXPHOS). However, sequential late-stage erythropoiesis is dependent on decreasing αKG-driven OXPHOS, and we find that isocitrate dehydrogenase 1 (IDH1) plays a central role

[*]Correspondence: pedro.gonzalez-menendez@igmm.cnrs.fr (P.G.-M.), taylorn4@mail.nih.gov (N.T.), kinet@igmm.cnrs.fr (S.K.).

AUTHOR CONTRIBUTIONS

P.G.-M., M.R., S.K., and N.T. conceived the study; P.G.-M., M.R., H.Y., R.D., J.P., L.O., S.T., V.D., C.M., M.S., V.S.Z., L.B., N.M., S.K., and N.T. were involved in study design; and P.G.-M., M.R., H.Y., R.D., J.P., L.O., S.T., C.M., M.D., A.-S.D., I.P., X.Q., P.-N.B., and S.K. performed experiments. All authors participated in data analysis. P.-G.M., S.K., and N.T. wrote the manuscript with important critical input from M.R., H.Y., L.O., S.T., X.A., V.D., M.S., V.S.Z., P.G.G., L.B., and N.M.

SUPPLEMENTAL INFORMATION

Supplemental Information can be found online at https://doi.org/10.1016/j.celrep.2021.108723.

in this process. IDH1 downregulation augments mitochondrial oxidation of αKG and inhibits reticulocyte generation. Furthermore, IDH1 knockdown results in the generation of multinucleated erythroblasts, a morphological abnormality characteristic of myelodysplastic syndrome and congenital dyserythropoietic anemia. We identify vitamin C homeostasis as a critical regulator of ineffective erythropoiesis; oxidized ascorbate increases mitochondrial superoxide and significantly exacerbates the abnormal erythroblast phenotype of IDH1-downregulated progenitors, whereas vitamin C, scavenging reactive oxygen species (ROS) and reprogramming mitochondrial metabolism, rescues erythropoiesis. Thus, an IDH1-vitamin C crosstalk controls terminal steps of human erythroid differentiation.

INTRODUCTION

Hematopoietic stem cell (HSC) numbers as well as their differentiation state are tightly regulated throughout the lifetime of an individual, allowing the sustained production of all mature blood lineages under physiological conditions. Circulating mature erythrocytes are a terminally differentiated product of HSCs that have undergone a series of lineage-fate engagements that gradually restrict their potential, resulting in a commitment to the erythroid lineage. Commitment defines the beginning of erythropoiesis; a three-stage process characterized by early erythropoiesis, terminal erythroid differentiation, and reticulocyte maturation. Early erythropoiesis is characterized by commitment of multilineage progenitor cells into erythroid progenitor cells, with proliferation and development into erythroid burst-forming unit cells, followed by erythroid colony-forming unit cells and proerythroblasts. Terminal erythroid differentiation begins with proerythroblasts differentiating in a stepwise manner to early then late basophilic erythroblasts, polychromatic erythroblasts, and orthochromatic erythroblasts that enucleate to become reticulocytes.

Erythropoiesis is a metabolically daunting process when evaluated at the level of cell numbers. In healthy adults, committed erythroid progenitors support the production of 2.4 million erythrocytes per second via a synchronized regulation of iron, glucose, fatty acid, and amino acid metabolism. Iron is indispensable for heme biosynthesis in erythroblasts (Oburoglu et al., 2016). The utilization of both glutamine and glucose in *de novo* nucleotide biosynthesis is a *sine qua non* for erythroid differentiation (Oburoglu et al., 2014), and glutamine-derived production of succinyl-coenzyme A (succinyl-CoA) is also required for the production of heme (Burch et al., 2018). Furthermore, amino acids regulate mTOR signaling (Chung et al., 2015) as well as lipid metabolism (Huang et al., 2018) during erythropoiesis. The critical nature of metabolism in erythroid differentiation is further highlighted by the recent identification of “metabolic regulators” as an erythropoietin (EPO)-induced phosphorylation target set (Held et al., 2020).

It is important though to note that terminal erythroid differentiation is a distinctive process; each mitosis results in the production of daughter cells that differ, morphologically and functionally, from their parent cells. This sequential maturation is tightly regulated at each stage of erythroid differentiation, associated with decreased cell size, enhanced chromatin condensation, progressive hemoglobinization, and changes in membrane organization and

transcriptome specificities (An et al., 2014; Hu et al., 2013; Li et al., 2014; Ludwig et al., 2019; Schulz et al., 2019). Moreover, during the late stages of mammalian terminal erythroid differentiation, erythroblasts expel their nuclei and lose all organelles, including mitochondria (Moras et al., 2017). Thus, the constraints of a late-stage terminally differentiating erythroblast differ significantly from that of an erythroid-committed progenitor early in erythroid development. Indeed, in mice, early-stage erythroid progenitors have been found to require mTORC1-mediated mitochondrial biogenesis and reactive oxygen species (ROS) production (Liu et al., 2017; Luo et al., 2017; Zhao et al., 2016), while terminal erythropoiesis requires that cells be protected from oxidative stress (Case et al., 2013; Filippi and Ghaffari, 2019; Hyde et al., 2012; Xu et al., 2019; Zhao et al., 2016).

Significant differences in murine versus human erythroid development have been documented, especially as relates to the diversity of erythroid progenitor subpopulations in human bone marrow (BM) (Gautier et al., 2020; Schulz et al., 2019; Yan et al., 2018). Furthermore, regarding oxidative stress, it is important to note that murine and human erythropoiesis differ dramatically as a function of vitamin C/ascorbate plasma concentrations and expression of the SLC2A1/GLUT1 transporter, shuttling dehydroascorbic acid (DHA) across the membrane and rapidly reducing it to ascorbate (reviewed by May et al., 2001). Indeed, humans exhibit a deficiency in vitamin C production, due to inactivation of L-gulono-γ-lactone oxidase (GLO), the enzyme that catalyzes the terminal step of L-ascorbic acid (AA) biosynthesis (Burns, 1957). While human erythrocytes express the highest level of the GLUT1 transporter, harboring greater than 200,000 molecules per cell (Helgerson and Carruthers, 1987; Mueckler, 1994), we found that erythroid GLUT1 expression is a specific feature of mammals that have lost the ability to synthesize AA from glucose (Montel-Hagen et al., 2008a, 2008b). This potential evolutionary compensation, and subsequent alterations in the ability of plasma vitamin C to scavenge ROS/reactive nitrogen species (RNS), make it critical to evaluate the stepwise changes that regulate the progression of human erythropoiesis.

Here, we demonstrate that during the early stages of human red blood cell development, erythroid progenitors exhibit increased oxidative phosphorylation (OXPHOS) activity. This correlated with the increased generation of the alpha-ketogluta-rate (αKG) TCA-cycle intermediate, generated by the anaplerotic utilization of glutamine, and a directly augmented OXPHOS. However, upon terminal differentiation of erythroblasts, mitochondrial biomass, OXPHOS, mitochondrial ROS, and superoxide production were all markedly decreased. Supraphysiological levels of αKG markedly attenuated terminal erythroid differentiation and enucleation. The impact of αKG was directly coupled to its role in mitochondrial metabolism, as enucleation was similarly inhibited by mitochondrial ROS and superoxide, induced by MitoParaquat (MitoPQ) or DHA. Moreover, enucleation was rescued by ROS scavengers, including vitamin C, glutathione (GSH), N-acetylcysteine (NAC), and vitamin E.

We identified the cytoplasmic isocitrate dehydrogenase 1 (IDH1) enzyme, catalyzing the interconversion between αKG and isocitrate, as a critical enzyme in this process. Lentiviral-mediated downregulation of IDH1, by significantly increasing mitochondrial metabolism and mitochondrial superoxide production, dramatically inhibited enucleation and resulted

in the generation of abnormal multinucleated erythroblasts. Notably, both αKG and DHA markedly exacerbated the negative impact of IDH1 downregulation, while the vitamin C antioxidant rescued erythroid differentiation. Indeed, the vitamin-C-mediated quenching of ROS in erythroblasts accelerated human erythroid differentiation. This effect was specific to an IDH1-vitamin C axis; inhibition of TET2 in late-stage erythroblasts did not attenuate enucleation. Thus, our data identify IDH1 as a critical regulator of redox homeostasis, promoting late-stage erythropoiesis. Furthermore, these results highlight the therapeutic potential of vitamin C in human erythropoiesis, especially under pathological conditions where ROS are increased and vitamin C levels are not sufficient to combat oxidative damage.

RESULTS

Early erythropoiesis is associated with augmented glutamine utilization and OXPHOS

As glutaminolysis is required for erythroid lineage specification (Oburoglu et al., 2014), we evaluated the utilization of glutamine during early stages of human erythropoiesis at day 4 following recombinant erythropoietin (rEPO) stimulation, a time point at which the erythroid markers CD36, CD71 (transferrin receptor), and glycophorin A (GlyA) are upregulated (Figure S1A). The anaplerotic contribution of glutamine can be evaluated by tracing glutamine labeled with heavy stable carbons and nitrogens ($^{13}C_5$ $^{15}N_2$). As shown in Figure 1A, the portion of glutamate derived from $^{13}C_5$ $^{15}N_2$ glutamine, a measure of glutaminase activity, increased significantly following erythropoietin-induced erythroid differentiation of human $CD34^+$ progenitors ($p < 0.05$; Figure 1A). Additionally, the contribution of labeled glutamine to the pool of glutamate ($^{13}C_5$ $^{15}N_1$ glutamate/$^{13}C_0$ glutamate) as well as the portion of $^{13}C_5$ labeled αKG increased significantly upon erythroid differentiation. This glutamate-derived generation of αKG was critical for OXPHOS in erythroid progenitors, as the oxygen consumption rate (OCR) was abrogated by the aminooxyacetic acid (AOA) transaminase inhibitor, blocking conversion of glutamate to αKG, and was completely restored by αKG supplementation (Figure 1B).

These data show that glutamine supports the tricarboxylic acid (TCA) cycle and downstream OXPHOS via the cataplerotic (utilization of αKG. As each stage of terminal erythroid differentiation is defined by a decreased cell size with the final stage of erythropoiesis resulting in enucleation and reticulocyte maturation, we assessed whether mitochondrial biomass and transmembrane polarization decrease following commitment of progenitors to an erythroid lineage fate. Indeed, both mitochondrial biomass and polarization, evaluated by MitoGreen and MitoRed staining, respectively, decreased massively upon erythroid differentiation, monitored as a function of day of differentiation (days 0–10) as well as on erythroblast subsets fluorescence-activated cell sorting (FACS) sorted on the basis of their CD49d/GLUT1 staining profiles ($p < 0.05$ to $p < 0.0001$; Figures 1C, 1D, and S1B).

These changes in mitochondrial biomass and polarization had functional consequences on terminal erythroid differentiation (Figure 1D). Erythroblasts at distinct stages of differentiation exhibited significant differences in their levels of OXPHOS, as estimated by their OCRs; basal OCR decreased from 146.9 ± 15.5 to 17.5 ± 0.6 pmol O_2/min between the proerythroblast and orthochromatic erythroblast stages of differentiation ($p < 0.0001$;

Figure 1E). Notably, the respiratory capacities of both polychromatic and orthochromatic subsets were minimal; neither of these terminal subsets exhibited a spare respiratory capacity, as measured by the ability of the cell to increase its respiration in response to an Carbonyl cyanide-4-(trifluoromethoxy)phenylhydrazone (FCCP)-mediated disruption of mitochondrial membrane potential (Figure 1E). Similarly, these differences were also detected with increasing time after EPO induction (Figure S1C). Consistent with a critical role for glutamine in the oxidative potential of the erythroblast, glutamine uptake was significantly higher in proerythroblasts and basophilic erythroblasts than in polychromatic/orthochromatic erythroblasts ($p < 0.01$; Figure 1F). Thus, in marked contrast with the high-energy state of early erythroid progenitors, terminal maturation results in a significant attenuation of glutamine uptake and an associated decrease in OXPHOS.

αKG increases mitochondrial function while negatively regulating terminal erythroid differentiation and enucleation

As decreased mitochondrial function of terminally differentiated erythroblasts was associated with decreased glutamine uptake, we evaluated whether αKG, the anaplerotic product of glutamine that enters into the TCA cycle, directly contributed to the erythroblast's respiratory capacity. Importantly, we found that αKG directly regulates the metabolic state of progenitors, as the injection of a cell-permeable αKG immediately augmented the maximal respiratory capacity of erythroblasts at both day 3 and day 7 of EPO induction ($p < 0.001$ and $p < 0.0001$; Figure 2A). This increase in OXPHOS did not alter the generation of $CD34^{-}CD36^{+}$ committed erythroid colony-forming unit (CFU-E) progenitors or $GlyA^{+}$ erythroblasts or the upregulation of CD36 or CD71 erythroid markers (Figures 2B and S2A). While αKG did not alter mitochondrial biomass or polarization at early stages of development (day 3; Figure S2B), it substantially affected these parameters when it was added only at later stages (from days 7 to 10). Mitochondrial biomass and polarization were significantly higher in αKG-supplemented late-stage erythroblasts than in control erythroblasts ($p < 0.01$ and $p < 0.001$; Figure 2C). Furthermore, progression from the $CD49d^{+}GLUT1^{+}$ basophilic erythroblast to the $CD49d^{-}Glut1^{+}$ orthochromatic stage was significantly inhibited by αKG ($p < 0.05$ and $p < 0.01$; Figure 2D). This phenomenon was also associated with a significantly attenuated level of enucleation, decreasing by 32% ± 7% and 52% ± 7% in the presence of αKG at days 10 and 14 of erythroid differentiation, respectively ($p < 0.001$ and $p < 0.01$; Figure 2D). Notably, this effect was specific to αKG and was not recapitulated by other TCA-cycle intermediates such as succinate or citrate (Figure S2C).

Augmented mitochondrial superoxide generation at the basophilic erythroblast stage abrogates terminal erythroid differentiation and enucleation

Generation of ROS within mitochondria is associated with the oxidative function of these organelles (Adam-Vizi and Tretter, 2013; Murphy, 2009), and αKG can directly contribute to ROS generation through the catalytic activity of αKG dehydrogenase (αKGDH) (Starkov et al., 2004; Tretter and Adam-Vizi, 2004). NADH produced by αKGDH also stimulates superoxide production by complex I of the electron transport chain (ETC; Figure 3A) (Adam-Vizi and Tretter, 2013; Murphy, 2009). We therefore evaluated whether addition of αKG, the substrate of αKGDH, alters the redox state of the cell. Direct measurement

of mitochondrial superoxide with the fluorescent MitoSOX indicator showed that αKG induced a 1.3-fold increase in superoxide ($p < 0.01$) as well as an overall increase of 1.3-fold in all mitochondrial ROS ($p < 0.001$), monitored as a function of DHR123 fluorescence (MitoROS) (Figure 3B).

These data suggested that the negative impact of αKG on erythroid maturation was linked to its role in altering the erythroblast redox state. We therefore assessed whether directly increasing mitochondrial superoxide would inhibit erythroid maturation. Erythroblasts were treated with MitoPQ, a newly synthesized paraquat compound that is targeted to the mitochondria by conjugation to the lipophilic tri-phenylphosphonium cation (Robb et al., 2015). This compound selectively increases superoxide production within mitochondria at 1,000-fold higher efficiency than untargeted paraquat (PQ) (Robb et al., 2015); within the mitochondria, mitoPQ^{2+} is reduced to the radical monocation at the flavin site of complex I and the monocation then reacts with O_2 to generate superoxide (O_2^-) (Figure 3C). MitoPQ dramatically increased mitochondrial superoxide (MitoSOX), MitoROS, and mitochondrial biomass (MitoGreen) in differentiating erythroblasts ($p < 0.01$ and $p < 0.05$; Figure 3D). The impact of both MitoPQ and αKG was specific to mitochondrial ROS, as total intracellular ROS levels were not significantly changed (Figures S3A and S3B). Notably, short-term MitoPQ treatment significantly altered late erythropoiesis, with a 25% ± 5% decrease in erythroblast enucleation ($p < 0.01$; Figure 3E).

To assess whether mitochondrial superoxide production has similar effects on erythroblasts at different stages of differentiation, we FACS-sorted early basophilic and late orthochromatic erythroblasts on the basis of their GLUT1/CD49d profiles. Representative cytospins are shown in Figure 3F. Notably, MitoPQ dramatically decreased the ability of basophilic erythroblasts to differentiate to reticulocytes, attenuating enucleation by 94% ± 3% ($p < 0.001$; Figure 3F). In contrast, the maturation of orthochromatic erythroblasts was not affected by MitoPQ treatment (Figure 3F). These data show that a cell type that exhibits only very minimal OXPHOS potential, such as an orthochromatic erythroblast (Figure 1E), is not sensitive to a drug whose impact is dependent on mitochondrial function. In contrast, selectively increasing superoxide production in the mitochondrial matrix of an early erythroblast significantly inhibits erythroid maturation, revealing the critical role of this pathway in the proper progression of erythroid differentiation.

DHA and vitamin C have opposing effects on erythroid maturation

As we found that oxidative stress, monitored as a function of mitochondrial superoxide production and OXPHOS, was associated with attenuated late-stage erythroid differentiation and enucleation, it was of interest to determine whether these parameters were directly responsible for these observed effects. Vitamin C has the potential to promote a redox environment, but its activity is countered by the oxidized form of vitamin C, DHA. The rapid reduction of intracellular DHA to vitamin C (Figure 4A) results in concomitant increases in endogenous ROS in tumor cell lines (Kc et al., 2005; Yun et al., 2015), but its role in erythroid cells is not known. Of note, DHA is transported via the GLUT1 glucose transporter, the most highly expressed transporter on human erythrocytes (Bianchi and Rose, 1986; Helgerson and Carruthers, 1987; May, 1998; Montel-Hagen et al., 2008b,

2009). We found that the addition of DHA significantly increased mitochondrial biomass and superoxide production in differentiating erythroblasts (Figure 4B). The DHA-induced increase in superoxide production was associated with a significant decrease in the enucleation of late-stage erythroblasts (from a mean of 40% ± 3% to 24% ± 3%; $p < 0.0001$; Figure 4C). Thus, under all tested conditions of superoxide production, enucleation of late-stage erythroblasts was severely attenuated.

Based on these data, it was important to evaluate whether vitamin C would have opposing effects on the redox state of erythroblasts and, subsequently, on erythroid maturation. As vitamin C is extremely labile, undergoing oxidation to DHA in culture media with a half-life of ~70 min (Yun et al., 2015), we evaluated the effect of AA-2-phosphate, which is resistant to spontaneous oxidation (Frikke-Schmidt and Lykkesfeldt, 2010; Hata and Senoo, 1989; Manning et al., 2013). This phosphorylated vitamin C molecule significantly enhanced the antioxidant capacity of the developing erythroblast, with a 23% ± 3% decrease in mitochondrial superoxide production ($p < 0.0001$; Figures 4D and S3C). To evaluate whether vitamin C can alter an imbalanced high oxidative state in erythroblasts, we tested its impact on αKG-induced metabolic changes in differentiating erythroblasts. Vitamin C significantly diminished mitochondrial superoxide production as well as mitochondrial biomass and polarization ($p < 0.0001$, $p < 0.01$, and $p < 0.05$; Figures 4E and S3D). Moreover, we found that while both αKG and MitoPQ significantly increased the percentages of erythroblasts in the S-G2/M phases of the cell cycle (with cell death remaining <15%), vitamin C decreased cell-cycle progression to control levels ($p < 0.05$ and $p < 0.01$; Figures 4F, S3E, and S3F).

Most importantly, vitamin C rescued the enucleation defect observed in these erythroblasts ($p < 0.0001$; Figure 4G). This effect was due to the reduced form of vitamin C; as only the long-acting derivative and not the labile form of vitamin C promoted enucleation (Figure S3G). Moreover, other ROS scavengers, including NAC (a thiol-containing antioxidant), GSH (the most abundant antioxidant), and Trolox (a water-soluble analog of vitamin E lacking the phytyl chain), recapitulated the actions of vitamin C, significantly augmenting terminal enucleation in the presence of αKG (Figure S4A). Similarly to the data shown above, highlighting the regulation of erythroid differentiation by mitochondrial metabolism at early erythroblast stages (Figure 3F), vitamin C significantly increased enucleation of sorted basophilic erythroblasts, but not orthochromatic erythroblasts (Figure S4B).

The ensemble of these data strongly suggests that the impact of vitamin C is due to its alteration of the redox state of the erythroblast. However, as autophagy is also a critical regulator of enucleation (Keerthivasan et al., 2011), we evaluated the impact of vitamin C following Spautin1-mediated inhibition of autophagy (Liu et al., 2011). As expected, Spautin significantly inhibited enucleation ($p < 0.01$), but vitamin C did not rescue this defect (Figure S5A), highlighting an autophagy-independent role of vitamin C in erythroid differentiation. Iron and its uptake as diferric transferrin by the transferrin receptor CD71 are also critical for erythroid differentiation (Kautz and Nemeth, 2014), and we therefore evaluated a potential crosstalk between iron and vitamin C. Interestingly, in the absence of transferrin, vitamin C did not increase enucleation in αKG-treated erythroblasts, but its presence (50 or 200 μg/mL) positively affected enucleation (Figure S5B). Thus, vitamin C

and other ROS scavengers decrease the redox state of erythroblasts, promoting enucleation under conditions of αKG-induced oxidative stress in a transferrindependent manner.

Vitamin C accelerates the erythroid differentiation of cord blood, peripheral blood, and BM progenitor cells

The ability of vitamin C to rescue erythroid differentiation under conditions of augmented oxidative stress led us to evaluate its potential to directly modulate erythroid differentiation of $CD34^+$ hematopoietic stem and progenitor cells (HSPCs) from different sources. $CD34^+$ progenitors from cord blood (CB), adult peripheral blood (PB), and BM were directly differentiated with rEPO. While BM-derived progenitors differentiated much more rapidly than CB- and PB-derived progenitors to an erythroid-committed CFU-E ($CD34^-CD36^+$), vitamin C did not alter the erythroid progenitor continuum (Figure S5C). In agreement with previous data (Yan et al., 2018), CB progenitors exhibited a delayed generation of $GlyA^+$ erythroblasts compared to PB and BM progenitors (Figure 5A). Notably, vitamin C significantly increased the percentages of $GlyA^+$ cells ($p < 0.05$) and increased maturation to a $GlyA^+CD105^-$ state by 2.1- ± 0.5-fold ($p < 0.01$, Figure 5A), without altering cell growth (Figure S5D). Furthermore, vitamin C resulted in an enhanced enucleation of erythroid progenitors generated from these three sources (Figure 5B). Thus, vitamin C significantly accelerates erythroid differentiation and enucleation of human $CD34^+$ progenitors, irrespective of their source of origin.

IDH1 activity regulates mitochondrial activity in differentiating erythroblasts

The data presented above demonstrated that conditions that increase mitochondrial activity in human erythroblasts, including ectopic αKG and MitoPQ, inhibit terminal erythroid differentiation. Under physiological conditions, αKG is mobilized in the mitochondria, where it can be converted to succinyl-CoA by αKGDH, producing ROS and the NADH that provides electrons for the ETC (Figure 6A). αKG can be generated from isocitrate in the mitochondria by IDH2/IDH3 and interconverted in the cytoplasm by IDH1. Interestingly, transcripts of all three enzymes are significantly reduced during erythroid differentiation, potentially suggesting a negative role for these pathways in late-stage erythroblasts (Figure S6A). As mitochondrial biomass is markedly decreased during erythroid differentiation, we evaluated the role of the cytoplasmic IDH enzyme, IDH1, in erythroid differentiation by an shIDH1-mediated approach. Using two independent short hairpin RNAs (shRNAs), shIDH1–1 and shIDH1–2, we detected a 36% ± 7% and 54% ± 5% reduction, respectively, and as such used shIDH1–2 in the differentiation experiments (Figure S6B).

Importantly, *IDH1* knockdown did not inhibit erythroid differentiation, as monitored by the generation of CFU-E, $GlyA^+$ erythroblasts or upregulation of the CD36 or CD71 erythroid markers (Figures 6B, S6C, and S6D). However, downregulating IDH1 resulted in a decreased expansion (Figure S6E) and significantly increased mitochondrial superoxide production, mitochondrial biomass, and polarization ($p < 0.01$; Figures 6C and S6F). In accord with these data, *IDH1* knockdown augmented the OXPHOS capacity of the cells, with a 3.0- and 3.7-fold increase in basal and maximal OCR levels, respectively (shIDH1–2 construct) (Figure 6D). Notably, the function of IDH1 appears to be substantially more critical for the differentiation of erythroid as compared to non-erythroid progenitors. The

percentages of progenitors transduced with an scramble shRNA (shControl) or shIDH1 lentiviral vector harboring the GFP reporter gene remained approximately stable over a 6-day period, with 47%–57% GFP^+ cells, in the absence of rEPO. These cells had a myeloid phenotype as shown by a $CD11b^+$, $CD33^+$, $CD13^+$ phenotype (Figure S6G). However, following rEPO-mediated erythroid induction, the percentages of shControl cells decreased by 24%, while the percentages of shIDH1-transduced cells decreased by 56% (Figure 6E).

To better understand the negative selection of erythroid progenitors with downregulated IDH1, we performed metabolomic and flux experiments following IDH1 knockdown. First, we found that at day 4 of IDH1 downregulation (~50%; Figure S6B), there was a mean decrease of αKG and citrate of 43% and 21%, respectively (Figure 6F). These data highlight the importance of the IDH1 enzyme in the generation of αKG and its interconversion to citrate. Furthermore, they demonstrate the role of glutamine metabolism in the generation of these intermediates in early erythroid progenitors (day 4); a mean of 75.1% and 69.0% of αKG and citrate harbored ^{13}C carbons from glutamine, respectively (Figure 6G). Several groups have also found that the relative ratio of αKG to citrate regulates differentiation, either by inhibiting (Carey et al., 2015; Vardhana et al., 2019) or priming (TeSlaa et al., 2016; Tischler et al., 2019) stem cell differentiation. In this regard, it is interesting to note that erythroid differentiation resulted in the loss of both αKG and citrate between days 4 and 7 of differentiation, with a mean loss of 87% and 68%, respectively (n = 2 biological experiments performed in triplicate; Figure 6G). These data point to a greater loss of αKG than citrate, consistent with a negative role of high αKG levels in late erythroid differentiation (Figure 2). Furthermore, following IDH1 downregulation, TCA intermediates were maintained at a higher level, with decreases in αKG and citrate of only 31% and 36%, respectively (Figure 6G). Thus, the premature inhibition of IDH1 alters the physiological loss of TCA-cycle intermediates upon erythroid differentiation.

Vitamin C rescues terminal erythroid differentiation in the absence of IDH1

Under conditions of IDH1 downregulation, mitochondrial metabolism was augmented, as shown by increased superoxide production and OXPHOS (Figures 6C and 6D). On the basis of these data, we hypothesized that *IDH1* knockdown would attenuate late-stage erythroid differentiation and enucleation, and this was indeed the case. Following transduction of $CD34^+$ HSPCs with a vector harboring an shIDH1 RNA, the emergence of $Glut1^+CD49^-$ orthochromatic erythroblasts was significantly decreased (shIDH1–2 construct, $p < 0.01$; Figure 7A). Furthermore, enucleation was decreased by 59% ± 2% (shIDH1–2 construct, $p < 0.0001$; Figure 7B), and this effect was detected even when IDH1 was downregulated at day 4 post-rEPO-induced differentiation (Figure S7A). Consistent with an impact of IDH1 on the redox state of the cell, both αKG and DHA exacerbated the effect of *IDH1* knockdown on erythroblast enucleation, from 47% ± 8% to 27% ± 8% and 24% ± 4%, respectively ($p < 0.01$ and $p < 0.05$; Figure 7C). Most importantly, vitamin C significantly increased enucleation under these conditions by 35% ± 13% ($p < 0.05$, Figure 7D). Intriguingly, other ROS scavengers, including NAC, GSH, and Trolox, did not increase enucleation, even though they were present throughout the differentiation period (Figure S7B). Importantly, vitamin C, but not NAC, GSH, or Trolox, decreased mitochondrial superoxide generation ($p < 0.05$; Figure S7C). Thus, collectively, these data show that IDH1-

induced decreases in mitochondrial OXPHOS are required for the later stages of terminal erythroid differentiation and enucleation. However, under conditions of decreased IDH1 expression, this negative effect can be counteracted by a vitamin-C-mediated modulation of the intracellular redox balance.

As αKG and vitamin C act as cofactors in supporting the dioxygenase activity of TET2, it was important to assess whether the effects that we detected here were coupled to their impact on TET2 activation (Inoue et al., 2016). However, if αKG served only to support the dioxygenase activity of TET2, then its presence would be expected to augment erythroid differentiation, while our data showed the opposite effect (Figure 2). To directly address this point and evaluate the role of an αKG/TET2 as compared to an αKG/IDH1 axis, we downregulated TET2 by an shRNA approach (Yan et al., 2017). TET2 levels decrease with differentiation ($p < 0.0001$; Figure S7D), but mRNA levels were further diminished by a mean of 55% by shRNA-mediated knockdown (Figure S7E). While this downregulation resulted in a significant delay in the generation of $GlyA^+$ terminal erythroblasts ($p < 0.0001$; Figure S7F), it did not delay enucleation when the shRNA-mediated knockdown of TET2 was performed at day 4 of differentiation (Figure 7E). Moreover, enucleation in shTET2-treated erythroid progenitors was not augmented by vitamin C (Figure 7E). These data strongly imply distinct roles for IDH1 and TET2 in regulating enucleation of late-stage erythroid progenitors.

Mutations in IDH1/IDH2 are strongly associated with myelodysplastic syndromes (MDSs) that are characterized by ineffective erythropoiesis (reviewed by Bejar and Steensma, 2014; Fenaux et al., 2014). The anemia that dominates the early course of MDS is associated with an aberrant erythroid differentiation marked by the generation of multinucleated erythroblasts (Abdel-Wahab and Levine, 2013). Notably, we found that *IDH1* knockdown increased the percentages of erythroblasts with abnormal multinucleated erythroblasts from 10% ± 1% to 23% ± 2% ($p < 0.05$; Figure 7F). Moreover, vitamin C markedly decreased the generation of these abnormal erythroblasts, not only in *IDH1*-knockdown erythroblasts but also in normal erythroblasts, to 4% ± 0.4% and 4% ± 0.2%, respectively ($p < 0.05$ and $p < 0.01$; Figure 7F). These data suggest that the multinucleated erythroblasts detected in MDS patients may be associated with an increased mitochondrial metabolism. Vitamin C, a redox scavenger, significantly attenuated the generation of these abnormal cells.

DISCUSSION

The generation of ROS and its intricate relationship with cellular redox homeostasis is a critical regulator of stem cell homeostasis. Notably, low ROS levels, associated with low mitochondrial biogenesis and activity, are necessary for HSC quiescence and self-renewal (Filippi and Ghaffari, 2019; Jang and Sharkis, 2007; Qian et al., 2016; Suda et al., 2011; Takubo et al., 2013; Tan and Suda, 2018; Vannini et al., 2016; Yu et al., 2013). Conversely, HSC division and differentiation occur under conditions that promote mitochondrial biogenesis and OXPHOS (Chen et al., 2008; Mantel et al., 2010; Maryanovich et al., 2015; Yu et al., 2013). In the context of erythropoiesis, it has been shown that early erythroid development requires induction of mitochondrial ROS, a consequence of OXPHOS (Liu et al., 2017; Zhao et al., 2016). Here, we show that glutamine

metabolism, via the anaplerotic contribution of αKG into the TCA cycle, directly increases OXPHOS in human erythroid precursors. This increased OXPHOS promoted erythroid commitment and early erythropoiesis, but terminal erythroid differentiation was dependent on the suppression of TCA-cycle-linked mitochondrial networks. Elevated intracellular αKG levels, with associated increased OXPHOS and ROS, inhibited late-stage erythroid maturation and enucleation.

Mechanistically, we identify the catalysis of αKG by the cytoplasmic IDH1 enzyme as a critical step in erythropoiesis; the negative repercussions of IDH1 downregulation in terminal erythroid differentiation was further exacerbated by elevated αKG levels. Furthermore, the impact of a mitochondria-targeted redox cycler, MitoPQ (Robb et al., 2015), highlights the importance of mitochondrial superoxide as a specific inhibitor of erythroblast maturation and enucleation. Interestingly, all tested ROS scavengers, including NAC, GSH, vitamin E, and vitamin C, rescued the αKG-mediated decrease in enucleation, but only vitamin C rescued enucleation following IDH1 downregulation. This is critical in the context of human erythroid differentiation, where the absence of ascorbate synthesis, resulting in 1 mg/kg recommended exogenous supplements for humans (Pauling, 1970), is significantly lower than the hepatic production rate of 200 mg/kg/day in vitamin-C-synthesizing animals (Chatterjee, 1973; Stone, 1979). Thus, scavenging by vitamin C is likely to be suboptimal. Indeed, we found that a stable vitamin C analog rescued human terminal erythroid differentiation and enucleation in all tested conditions of oxidative stress.

Ascorbate, transported by the SVCT1/SLC23A1 and SVCT2/SLC23A2 solute carriers, regulates whole-body homeostasis of vitamin C and protection to oxidative stress, respectively (Savini et al., 2008; Tsukaguchi et al., 1999; Wilson, 2005). While vitamin C has been shown to enhance erythropoiesis in hemodialysis patients with refractory anemia (Attallah et al., 2006; Gastaldello et al., 1995; Seibert et al., 2017; Sirover et al., 2008), other studies have found that ascorbate induces hemolysis of mature erythrocytes (Zhang et al., 2016). These apparent discrepancies are likely due to the oxidation state of vitamin C. The loss of a single electron from ascorbate results in the generation of an unstable ascorbate radical, which can then lose a second electron to generate DHA (Padayatty and Levine, 2016). Unlike vitamin C, the two-electron oxidized DHA intermediate is transported by the GLUT1 glucose transporter (Bianchi and Rose, 1986; McNulty et al., 2005; Rumsey et al., 1997, 2000; Vera et al., 1993). Thus, cellular uptake of the reduced and oxidized forms of vitamin C is regulated, at least in part, by the expression of their specific transporters. SVCT2 is expressed at very high levels on HSCs, with levels decreasing as a function of erythroid development and differentiation (Agathocleous et al., 2017). Conversely, GLUT1 is upregulated during human terminal erythroid differentiation (Montel-Hagen et al., 2008b; Mueckler, 1994), promoting DHA transport (May, 1998; Montel-Hagen et al., 2008b, 2009). Thus, during intermediate steps of HSPC development, both ascorbate and DHA can potentially be transported into the cell.

One of the difficulties in studying ascorbate function is its stability. Previous research showed that freshly prepared minimum essential medium α (αMEM) culture media, but not liquid αMEM, supported T cell differentiation from hematopoietic progenitors; the difference between these formulations was due to the lability of vitamin C in the latter

(Manning et al., 2013). Furthermore, several groups found that the negative impact of vitamin C on the growth of cancer cells was actually due to the GLUT1-mediated uptake of DHA, resulting in the accumulation of ROS and subsequent cell death (Yun et al., 2015; Zhang et al., 2016).

Indeed, we similarly found that the standard labile form of L-ascorbate markedly decreased erythroblast maturation and enucleation, even in the absence of ascorbate oxidase. However, under conditions where erythroid differentiation was performed in the presence of the stable ascorbate 2-phosphate analog (Hata and Senoo, 1989; Frikke-Schmidt and Lykkesfeldt, 2010; Takamizawa et al., 2004), erythroid differentiation was enhanced. Thus, care must be taken in evaluating studies using the conventional labile ascorbate, as it may not be maintained in a reduced state.

Ascorbic acid has also gained prominence as an anti-cancer therapeutic modality because of its ability to alter the activity of the Tet2 demethylase (Shenoy et al., 2018). Loss of function mutations in *TET2* are one of the most frequent events in myeloid dysplasia and leukemias (Bejar et al., 2011; Busque et al., 2012; Delhommeau et al., 2009; Kosmider et al., 2011). The initiation of demethylation by the TET family of dioxygenases occurs via the introduction of the intermediate mark 5-hydroxymethyl-cytosine (5hmC), and this function is dependent on several cofactors, including ascorbate, αKG, ferrous iron, and oxygen (Chen et al., 2013; Dang et al., 2009). Indeed, recent studies have shown that ascorbate is able to compensate for TET2 deficiency and suppress leukemogenesis, albeit via both TET2-dependent and TET2-independent mechanisms (Agathocleous et al., 2017; Cimmino et al., 2017). A crosstalk between ascorbate and TET2 in the metabolic status of a hematopoietic progenitor is suggested by the finding that wild-type TET2 protects murine erythroblasts from oxidative stress (Guo et al., 2017). Moreover, downregulation of TET2 in human erythroid progenitors negatively regulated human erythropoiesis in a manner that was independent of any detectable alterations in 5-methyl-cytosine (5mC) levels (Qu et al., 2018; Yan et al., 2017). These data are in agreement with independent studies showing that terminal erythroid differentiation requires that erythroblasts be protected from oxidative stress (Case et al., 2013; Filippi and Ghaffari, 2019; Hyde et al., 2012; Xu et al., 2019; Zhao et al., 2016).

Our study highlights the importance of ascorbate in regulating the redox state of human erythroid progenitors, especially under conditions of altered oxidative metabolism. Increases in intracellular αKG and decreases in cytoplasmic IDH1 both augmented oxidative stress and diminished erythroid maturation. IDH1, like Tet2, is mutated in a high percentage of MDS patients (Kosmider et al., 2010; Wang et al., 2017), with anemia dominating the early course of disease. Moreover, recent studies have highlighted the potential for vitamin C to promote the differentiation of IDH1-mutated AML progenitors (Mingay et al., 2018). Our data show that even in the absence of mutation, low levels of wild-type IDH1 suppress late erythroid differentiation. While the specific role of IDH1 in OXPHOS has not yet been fully delineated, it is interesting to note that IDH1 downregulation in neuronal cells resulted in an increase in ROS (Calvert et al., 2017). Furthermore, mutation of IDH1, but not IDH2, has been found to increase OXPHOS in transformed cells (Grassian et al., 2014), and wild-type

IDH1 regulates the reductive carboxylation of αKG for *de novo* lipogenesis (Calvert et al., 2017; Metallo et al., 2011).

IDH-regulated αKG production has also been shown to regulate cell fate and differentiation by modulating epigenetic marks via Tet2-induced changes in global histone and DNA demethylation (Carey et al., 2015; TeSlaa et al., 2016; Tischler et al., 2019; Xiao et al., 2012). Notably, under the conditions of erythroid differentiation studied here, αKG levels attenuated terminal erythroid differentiation and late-stage erythropoiesis, while a second TET2 cofactor, ascorbate, exhibited an opposing effect, enhancing and accelerating terminal differentiation. Other agents, such as oxidized ascorbate and MitoPQ, attenuated erythroid differentiation by inducing oxidative stress. Furthermore, while TET2 downregulation delayed early erythroblast differentiation, it did not negatively impact terminal differentiation and enucleation. Together, these data strongly suggest complementary roles for TET2 and IDH1, with the latter playing a critical role in late-stage human erythropoiesis via its impact on redox homeostasis.

These data may promote mechanistic insights into inherited hematologic disease. Like MDS patients, a feature that characterizes patients with congenital dyserythropoietic anemia is the presence of multinucleated or multi-lobulated erythroblasts (Crookston et al., 1969; Goasguen et al., 2018; Iolascon et al., 1996). IDH1 knockdown resulted in a significant augmentation in the percentage of abnormal multinucleated orthochromatic erythroblasts, and even more importantly, ascorbate reduced these levels back to baseline. Thus, these data provide the first evidence that the abnormal erythroblast morphology observed in diverse dyserythropoietic diseases may be coupled to oxidative stress. Furthermore, our data suggest that antioxidant treatment of these disorders in humans, a species with suboptimal redox capacity (Johnson et al., 2008), with stable ascorbate analogs could potentially restore redox homeostasis, quenching ROS and subsequently rescuing defective late-stage erythropoiesis.

STAR★METHODS

RESOURCE AVAILABILITY

Lead contact—Further information and requests for resources and reagents should be directed to and will be fulfilled by the Lead Contact, Naomi Taylor (taylorn4@mail.nih.gov).

Materials availability—This study did not generate new unique reagents. All lentiviral vectors generated in this study are available on request.

Data and code availability—This study did not generate datasets or code.

EXPERIMENTAL MODELS AND SUBJECT DETAILS

CD34$^+$ cell isolation and *ex vivo* differentiation assays.—All studies involving human samples were conducted in accordance with the declaration of Helsinki. CD34$^+$ cells were isolated from umbilical cord blood within 24h of vaginal delivery of full-term infants after informed consent and approval by the “Committee for the Protection of Persons” (IRB) of the University Hospital of Montpellier. Peripheral blood from leukoreduction filters and

bone marrow were obtained from deidentified donors at the New York Blood Center and the North Shore-LIJ Health System, respectively, after informed consent and approval from the respective IRBs. Approximately 60 UCB, 10 PB and 6 BM samples were used in this study. Samples did not contain any identifiers including sex, race, or ethnic origin. All samples were split such that they were used in all experimental groups. As such, there was no need to use any specific criteria to allocate biological samples to experimental groups. For the vast majority of experiments, at least 3 biological samples were used. For experiments presented in Figures 1A, 6F, and 6G, 2 biological samples were employed and technical triplicates were evaluated for both samples.

$CD34^+$ cells (1×10^5 cells/ml) were expanded in StemSpan H3000 media (StemCell Technologies Inc) supplemented with StemSpam CC100 (StemCell Technologies Inc) at 37°C with a humidified 5% CO_2 atmosphere. Cells were plated in 24-well *Nunclon Delta surface plates (Nunc, Thermo Fisher Scientific).* After 4 days of expansion, cells were differentiated in IMDM medium (Invitrogen) supplemented with human holo-transferrin (200 mg/L, Sigma-Aldrich), human insulin (10 mg/L, Sigma-Aldrich), rhuSCF (10 ng/ml, Amgen), rhuIL-3 (1 ng/ml, R&D Systems). Erythropoiesis was induced by addition of 3 U/ml recombinant human erythropoietin (rEPO; Eprex, Janssen-Cilag). In some experiments, $CD34^+$ cells were not expanded and erythropoiesis was directly induced after selection (data in Figure 5). Cytokines were supplemented every 3–4 days at the same time that media was renewed. Cells were centrifuged at 300 g for 10min at RT and then resuspended in fresh media to maintain cell concentrations between 0.1 and 1.5×10^6 cells/ml. In some experiments, progenitors were differentiated in the presence of 3.5 mM cell permeable dimethyl α-ketoglutarate (DMK, Sigma-Aldrich), 5 mM diethylsuccinate (Sigma Aldrich), 8 mM citrate (Sigma-Aldrich), 1 mM aminooxyacetate (AOA, Sigma-Aldrich), 50 μM MitoParaquat (MitoPQ, Abcam), 1 mM L-ascorbic acid (AA, Sigma-Aldrich), 100 μM 2-phospho-L-ascorbic acid (Vit C, Sigma-Aldrich), 100 μM N-acetylcysteine (NAC, Sigma-Aldrich), 100 μM reduced glutathione (GSH, Sigma-Aldrich), 100 μM of the water-soluble analog of vitamin E (TROLOX, Sigma Aldrich), or 10 μM of specific and potent autophagy inhibitor-1 (Spautin-1, Sigma-Aldrich). Ascorbate oxidase (1 U/mL, Sigma-Aldrich) was used to completely oxidize L-ascorbic acid to DHA in culture medium before treating the cells. Drugs were freshly added after every media change. In experiments where cells were co-cultured with α-KG (DMK, 3.5 mM) in the presence of antioxidants, α-KG was administered 2 hours after the addition of the corresponding antioxidant. As MitoPQ and TROLOX were dissolved in DMSO, control conditions included cultures using the same concentration of DMSO (0.05 and 0.1%, respectively).

METHODS DETAIL

Cytospin preparation—Cytospins were prepared on glass slides (5×10^4 cells in 200 μL of PBS), using the Thermo Scientific Shandon 4 Cytospin (300 g for 5 min). Slides were stained with May-Grunwald solution (Sigma-Aldrich) for 5 min, rinsed in 40 mM Tris buffer for 90 s, and subsequently stained with Giemsa solution (Sigma-Aldrich) for 15 minutes. Cells were imaged using a Leica DM2000 inverted microscope under 100 × objective magnification.

Flow cytometry—Expression of the CD34, CD36, CD49d, CD71, CD105 (Ashley et al., 2020), Glycophorin A, IL3R, CD11b, CD13, and CD33 surface markers was monitored on 1–2×10^5 cells using the appropriate fluorochrome-conjugated monoclonal antibodies at a 1:100 dilution (mAb), except for CD36-APC and CD71-AF750 mAbs that were used at a 1:200 and 1:500 dilution, respectively (Beckman Coulter, Becton Dickinson, eBiosciences), in a total volume of 100 μls as previously described (Hu et al., 2013; Schulz et al., 2019). Cells were incubated in the dark for 20 minutes in PBS containing 2% FBS at 4°C and then washed once in the same medium at 300 g for 10 min prior to evaluation. GLUT1 expression was monitored by binding to its retroviral envelope ligand (RBD) fused to eGFP (1:25 dilution in 50 μls; Metafora biosystems) or to the RBD-rFc fusion protein (1:25 dilution in 50 μls) for 30 minutes in PBS containing 2% FBS at 37°C followed by staining with an Alexa Fluor 405-coupled anti-rabbit IgG antibody (1:100 dilution in 100 μls) at 4°C as previously reported (Kim et al., 2004; Kinet et al., 2007; Manel et al., 2003; Swainson et al., 2005). Mitochondrial biomass was assessed in a total volume of 50 μls by MitoTrackerGreen or MitoTrackerDeepRed staining (20 nM; Invitrogen, Molecular Probes), while mitochondrial transmembrane potential levels were monitored by staining with MitoTrackerRed (50 nM; Invitrogen, Molecular Probes). Mitochondrial superoxide production, mitochondrial ROS levels and total ROS levels were assessed by staining with MitoSOX, Dihydrorodamine 123 and CM-H2DCFDA, respectively (5 μM; Invitrogen, Molecular Probes). Incubations were performed in the dark for 20 minutes in PBS + 2% FBS at RT. Enucleation was evaluated by staining with the SYTO16 or SYTO60 nucleic acid stain (1 μM and 0.5 μM, Invitrogen, Molecular Probes) for 15 minutes in PBS + 2% FBS at RT. Cell cycle analysis was performed by staining for DNA using 50 μg/mL propidium iodide (PI; Sigma-Aldrich) following permeabilization in 100 μls of 0.1% Triton X-100. To assess cell death, cells were incubated with PI (10 μg/ml). Cell sorting was performed on a FACSARIA high-speed cell sorter (BD Biosciences) and analyses were performed on a FACS-Canto II (BD Biosciences) cytometers. A minimum of 10,000 events were recorded for each staining. Data analyses were performed using FlowJo software (Tree Star, Ashland, OR).

Virus production and transduction of $CD34^+$ progenitor cells—Lentiviral pLKO.1 plasmids harboring shRNAs directed against *IDH1* (shRNA IDH1–1: Clone ID: TRCN0000027284 and shRNA IDH1–2: ID: TRCN0000312463) and lentiviral TRC2-pLKO plasmid harboring shRNA against TET2 (ID: TRCN0000418976) (Yan et al., 2017) were obtained from Sigma-Aldrich. Cells were transduced with the shRNA IDH1–1 lentiviral plasmid, the shRNA IDH1–2 plasmid or the shRNA TET2 plasmid where the 714bp sequence encoding for EGFP was inserted in place of the puromycin gene at the unique BamHI and KpnI restriction sites. Virions were generated by transient transfection of 293T cells (2–3×10^6 cells/100mm plate in 7 mL DMEM) with these vectors (10 mg) together with the Gag-Pol packaging construct PsPax2 (5 mg) and a plasmid encoding the VSV-G envelope, pCMV-VSV-G (2.5 mg), as described previously (Loisel-Meyer et al., 2012). Cells were transfected for at least 18 hours, and transfection efficiency was verified by monitoring GFP fluorescence by microscopy. Viral supernatant was harvested 24 hours post-transfection and virions were concentrated by overnight centrifugation at 4°C at 1,500 g (with no break). Virions were resuspended in approximately 20 ml of RPMI with 10% FBS

(per plate of cells), aliquoted and stored at −80°C. Titers were determined by serial dilutions of virus preparations on Jurkat cells and are expressed as Jurkat transducing units (TU/ml).

Prior to transduction of $CD34^+$ hematopoietic stem and progenitor cells (HSPCs), cells were expanded for 3 days in StemSpan medium (Stem cell Technologies Inc) supplemented with 5% fetal bovine serum (FBS), 25 ng/ml rhuSCF (Amgen), 10 ng/ml rhuIL-3 and 10 ng/ml rhuIL-6 (R&D) at 37°C with a humidified 5% CO_2 atmosphere. 5×10^5 cells were then exposed to viral supernatants containing 4.8×10^5 TU to 9.9×10^5 TU (representing a multiplicity of infection of 1–2). After 72h of transduction, $CD34^+$ cells (1×10^5 cells/ml) were cultured in presence of rEPO (3 U/ml) to induce erythropoiesis. Transduction efficiency was monitored as a function of GFP expression or after puromycin selection at 72h post-transduction, as per the lentiviral vector. In some experiments, cells were transduced at day 4 of erythroid differentiation (i.e., at day 4 following addition of EPO) under the same conditions as described above, and transduction efficiency was monitored at day 7 of differentiation.

Quantitative real time PCR—Total RNA was isolated at the indicated time points and cDNA was synthetized using the RNeasy Mini kit and the QuantiTect™ Reverse Transcription Kit (QIAGEN) as per the manufacturer's instructions. Quantitative PCR of cDNAs was performed using the Quantitect SYBR green PCR Master mix (Roche) with 10 ng of cDNA (by NanoDrop) and 0.5 μM primers in a final volume of 10μl. Primer sequences are as follows: *IDH1*: 5′-GGGTTGGCCTTTGTATCTGA-3′ (forward) / 5′- TTTACAGGCCCAGATGAAGC –3′ (reverse); IDH2: 5′-TGGCTCAGGTCCTCAAGTCT-3′ (forward) / 5′-CTCAGCCTCAATCGTCTTCC-3′ (reverse); IDH3a: 5′-GCGCAAAA CATTTGACCTTT-3′ (forward) / 5′-TGCACGACTCCATCAACAAT-3′ (reverse); TET2: 5′-AGCAGCAGCCAATAGGACAT-3′ (forward) / 5′-AGGTTCTGTCTGGCAAATGG-3′ (reverse); and b-actin: 5′-GTCTTCCCCTCCATCGTG-3′ (forward) / 5′-TTCTCCATGTCGTCCC AG-3′ (reverse). Amplification of cDNAs was performed using the LightCycler 480 (Roche). Cycling conditions included a denaturation step for 5 min at 95°C, followed by 40 cycles of denaturation (95°C for 10 s), annealing (63°C for 10 s) and extension (72°C for 10 s). After amplification, melting curve analysis was performed with denaturation at 95°C for 5 s and continuous fluorescence measurement from 65°C to 97°C at 0.1°C/s. Each sample was amplified in triplicate. Data were analyzed by LightCycler® 480 Software (Version 1.5) and Microsoft Excel. Relative expression was calculated by normalization to β-actin as indicated (delta-Ct). Realtime PCR CT values were analyzed using the 2(-Delta Delta C(T)) method to calculate fold expression (ddCt).

Mass spectrometry (LC-MS)—For profiling of intracellular metabolites, 10^6 cells were incubated in IMDM medium without glutamine and were supplemented with 2mM uniformly labeled $^{13}C_5$-$^{15}N_2$ glutamine (Cambridge Isotope Laboratories) for 6 hours (Figure 1A) or 18 hours (Figures 6F and 6G). Cells were rapidly washed in ice-cold PBS, centrifuged twice (400 g for 4 min), and metabolites were extracted in a solution of 50% methanol, 30% acetonitrile, 20% water after shaking for 20 min at 4°C. The solutions were then recentrifuged for 10 min at 16,000 g at 4°C. The volume of the extraction solution

was adjusted to achieve a constant ratio of 2×10^6 cells/ml. Alternatively, the peak areas resulting from the intracellular samples were normalized to the number of cells obtained at the end of the incubation period in parallel wells. Supernatants were stored at −20°C until analysis. Samples were analyzed by HPLC-MS as described previously (Vande Voorde et al., 2019). Data were analyzed with Xcalibur 2.2, LCquan 2.7 and TraceFinder 4.1 software (Thermo scientific). Samples were performed in triplicate, and at least 2 different biological samples were evaluated for each condition.

Seahorse analysis—Oxygen consumption rates (OCR) and extracellular acidification rates (ECAR) were measured using the XFe-96 Extracellular Flux Analyzer (Seahorse Bioscience, Agilent). The calibration plate was filled with 200 µL Milli-Q water per well and kept at 37°C overnight. At least 2 hours prior to the assay, water was replaced by 200 µL XF calibrant (Agilent)/ well. Culture plates were treated with 20 µl/well of 0.1mg/mL of Poly-D-Lysine for at least 1 hour at RT. Poly-D-Lysine (Sigma-Aldrich) solution was then removed and plates was washed twice with 200 µL Milli-Q water/well, dried, and kept at 4°C until the assay was performed. Cells (2.5×10^5) were placed in 50 µL XF medium (non-buffered DMEM containing 10 mM glucose and 2 mM GlutaMax, pH 7.3–7.4, Agilent), centrifuged in a carrier tray (300 g for 3min with no break), and incubated for 30 min at 37°C. An additional 130 µL XF medium was added during the calibration time (20–30 min at 37°C). Cells were monitored in basal conditions and in response to oligomycin (1 mM; Sigma-Aldrich), FCCP (1 µM; Sigma-Aldrich), rotenone (100 nM, Sigma-Aldrich) and antimycin A (1 µM; Sigma-Aldrich). In some experiments, αKG (DMK, final concentration of 3.5 mm) was injected directly into the well before the sequential addition of oligomycin, FCCP, rotenone and antimycin A during the Mito Stress Test. Wave software (Agilent) was employed for running the Seahorse assay and analysis. Samples were performed at least in triplicate and generally 5–6 points per experiment and at least 3 independent experiments.

Glutamine uptake assays—Cells (5×10^5) were washed twice in 1.5 mL of PBS containing 2%FBS at 400 g for 4 min at RT, and starved for glutamine by incubation at 37°C in 30 µl glutamine-free RPMI for 30 min. Radiolabeled glutamine-L-[3,4-^{3}H(N)] (Perkin Elmer) was added to a final concentration of 0.5 µM (0.5 mCi/mL in a total volume of 50 µL). Cells were incubated for 10 min at room temperature, washed twice in cold PBS containing 2%FBS (1000 g, 3 min), and solubilized in 500 µL of a 0.1% SDS solution. Radioactivity was measured in 4.5 mL liquid scintillation (Perkin Elmer) using a Hidex 300 SL counter. Each independent experiment was performed in triplicate.

QUANTIFICATION AND STATISTICAL ANALYSIS

Data are represented as individual values or means. Error bars represent the standard error of the mean (SEM). Data were analyzed with GraphPad Software (GraphPad Prism), and *P*-values were determined by one-way ANOVA (Tukey's post hoc test) or t tests, as indicated in the corresponding text and figure legends. Two-tailed t tests were used in all figures except for Figure 6F where a one-tailed t test was used. Tests were paired or unpaired as indicated and a normal distribution was used in all experiments. All statistical details of experiments can be found in the figure legends. Significance is indicated as * $p < 0.05$, **p

< 0.01, ***p < 0.001 and ****p < 0.0001 as evaluated by GraphPad. The graphical abstract was created using BioRender and Servier Medical Art.

Supplementary Material

Refer to Web version on PubMed Central for supplementary material.

ACKNOWLEDGMENTS

We thank all members of our laboratories for discussions and scientific critique. We are grateful to Myriam Boyer of Montpellier Rio Imaging for support in cytometry experiments. We are indebted to the Tissue Donation Program at Northwell Health for providing access to BM samples. We thank the Unité of Thérapie Cellulaire and the hospital clinics of Clémentville and Saint-Roch (Montpellier, France) for their generous efforts in providing access to CB samples. We also thank Catherine Winchester for critical reading of the manuscript. P.G.-M. was supported by a fellowship from the Clarin-COFUND EU Program (Principado de Asturias, Spain), M.R. was supported by a fellowship from GR-Ex, and L.O. was supported by Ligue and ARC fellowships. S.T. is supported by funding from Cancer Research UK (C596/A17196 and A23982). This work was supported by generous funding from the NIH (grant DK32094 to P.G.G., N.M., S.K., and N.T. and grants HL144436 and HL152099 to L.B.); FRM, ARC, and French national (ANR) research grants (NutriDiff); and the French laboratory consortiums (Labex) EpiGenMed and GR-Ex. N.T. is presently supported by the NCI Intramural Program.

DECLARATION OF INTERESTS

M.S. and S.K. are inventors on a patent describing the use of a ligand for evaluation of GLUT1 expression (N.T. gave up her rights). M.S. is a co-founder of METAFORA Biosystems, focusing on metabolite transporters under physiological and pathological conditions, and is head of the scientific board.

REFERENCES

Abdel-Wahab O, and Levine RL (2013). Mutations in epigenetic modifiers in the pathogenesis and therapy of acute myeloid leukemia. Blood 121, 3563–3572. [PubMed: 23640996]

Adam-Vizi V, and Tretter L (2013). The role of mitochondrial dehydrogenases in the generation of oxidative stress. Neurochem. Int. 62, 757–763. [PubMed: 23357482]

Agathocleous M, Meacham CE, Burgess RJ, Piskounova E, Zhao Z, Crane GM, Cowin BL, Bruner E, Murphy MM, Chen W, et al. (2017). Ascorbate regulates haematopoietic stem cell function and leukaemogenesis. Nature 549, 476–481. [PubMed: 28825709]

An X, Schulz VP, Li J, Wu K, Liu J, Xue F, Hu J, Mohandas N, and Gallagher PG (2014). Global transcriptome analyses of human and murine terminal erythroid differentiation. Blood 123, 3466–3477. [PubMed: 24637361]

Ashley RJ, Yan H, Wang N, Hale J, Dulmovits BM, Papoin J, Olive ME, Udeshi ND, Carr SA, Vlachos A, et al. (2020). Steroid resistance in Diamond Blackfan anemia associates with p57Kip2 dysregulation in erythroid progenitors. J. Clin. Invest. 130, 2097–2110. [PubMed: 31961825]

Attallah N, Osman-Malik Y, Frinak S, and Besarab A (2006). Effect of intravenous ascorbic acid in hemodialysis patients with EPO-hyporesponsive anemia and hyperferritinemia. Am. J. Kidney Dis. 47, 644–654. [PubMed: 16564942]

Bejar R, and Steensma DP (2014). Recent developments in myelodysplastic syndromes. Blood 124, 2793–2803. [PubMed: 25237199]

Bejar R, Stevenson K, Abdel-Wahab O, Galili N, Nilsson B, Garcia-Manero G, Kantarjian H, Raza A, Levine RL, Neuberg D, and Ebert BL (2011). Clinical effect of point mutations in myelodysplastic syndromes. N. Engl. J. Med. 364, 2496–2506. [PubMed: 21714648]

Bianchi J, and Rose RC (1986). Glucose-independent transport of dehydroascorbic acid in human erythrocytes. Proc. Soc. Exp. Biol. Med. 181, 333–337. [PubMed: 3945643]

Burch JS, Marcero JR, Maschek JA, Cox JE, Jackson LK, Medlock AE, Phillips JD, and Dailey HA Jr. (2018). Glutamine via α-ketoglutarate dehydrogenase provides succinyl-CoA for heme synthesis during erythropoiesis. Blood 132, 987–998. [PubMed: 29991557]

Burns JJ (1957). Missing step in man, monkey and guinea pig required for the biosynthesis of L-ascorbic acid. Nature 180, 553. [PubMed: 13477232]

Busque L, Patel JP, Figueroa ME, Vasanthakumar A, Provost S, Hamilou Z, Mollica L, Li J, Viale A, Heguy A, et al. (2012). Recurrent somatic TET2 mutations in normal elderly individuals with clonal hematopoiesis. Nat. Genet. 44, 1179–1181. [PubMed: 23001125]

Calvert AE, Chalastanis A, Wu Y, Hurley LA, Kouri FM, Bi Y, Kachman M, May JL, Bartom E, Hua Y, et al. (2017). Cancer-associated IDH1 promotes growth and resistance to targeted therapies in the absence of mutation. Cell Rep. 19, 1858–1873. [PubMed: 28564604]

Carey BW, Finley LW, Cross JR, Allis CD, and Thompson CB (2015). Intracellular alpha-ketoglutarate maintains the pluripotency of embryonic stem cells. Nature 518, 413–416. [PubMed: 25487152]

Case AJ, Madsen JM, Motto DG, Meyerholz DK, and Domann FE (2013). Manganese superoxide dismutase depletion in murine hematopoietic stem cells perturbs iron homeostasis, globin switching, and epigenetic control in erythrocyte precursor cells. Free Radic. Biol. Med. 56, 17–27. [PubMed: 23219873]

Chatterjee IB (1973). Evolution and the biosynthesis of ascorbic acid. Science 182, 1271–1272. [PubMed: 4752221]

Chen C, Liu Y, Liu R, Ikenoue T, Guan KL, Liu Y, and Zheng P (2008). TSC-mTOR maintains quiescence and function of hematopoietic stem cells by repressing mitochondrial biogenesis and reactive oxygen species. J. Exp. Med. 205, 2397–2408. [PubMed: 18809716]

Chen Q, Chen Y, Bian C, Fujiki R, and Yu X (2013). TET2 promotes histone O-GlcNAcylation during gene transcription. Nature 493, 561–564. [PubMed: 23222540]

Chung J, Bauer DE, Ghamari A, Nizzi CP, Deck KM, Kingsley PD, Yien YY, Huston NC, Chen C, Schultz IJ, et al. (2015). The mTORC1/4E-BP pathway coordinates hemoglobin production with L-leucine availability. Sci. Signal. 8, ra34. [PubMed: 25872869]

Cimmino L, Dolgalev I, Wang Y, Yoshimi A, Martin GH, Wang J, Ng V, Xia B, Witkowski MT, Mitchell-Flack M, et al. (2017). Restoration of TET2 function blocks aberrant self-renewal and leukemia progression. Cell 170, 1079–1095.e20. [PubMed: 28823558]

Crookston JH, Crookston MC, Burnie KL, Francombe WH, Dacie JV, Davis JA, and Lewis SM (1969). Hereditary erythroblastic multinuclearity associated with a positive acidified-serum test: a type of congenital dyserythropoietic anaemia. Br. J. Haematol. 17, 11–26. [PubMed: 5807784]

Dang L, White DW, Gross S, Bennett BD, Bittinger MA, Driggers EM, Fantin VR, Jang HG, Jin S, Keenan MC, et al. (2009). Cancer-associated IDH1 mutations produce 2-hydroxyglutarate. Nature 462, 739–744. [PubMed: 19935646]

Delhommeau F, Dupont S, Della Valle V, James C, Trannoy S, Massé A, Kosmider O, Le Couedic JP, Robert F, Alberdi A, et al. (2009). Mutation in TET2 in myeloid cancers. N. Engl. J. Med. 360, 2289–2301. [PubMed: 19474426]

Fenaux P, Haase D, Sanz GF, Santini V, Buske C, and Group EGW (2014). Myelodysplastic syndromes: ESMO Clinical Practice Guidelines for diagnosis, treatment and follow-up. Ann. Oncol. 25, 57–69. [PubMed: 24276029]

Filippi MD, and Ghaffari S (2019). Mitochondria in the maintenance of hematopoietic stem cells: new perspectives and opportunities. Blood 133, 1943–1952. [PubMed: 30808633]

Frikke-Schmidt H, and Lykkesfeldt J (2010). Keeping the intracellular vitamin C at a physiologically relevant level in endothelial cell culture. Anal. Biochem. 397, 135–137. [PubMed: 19782654]

Gastaldello K, Vereerstraeten A, Nzame-Nze T, Vanherweghem JL, and Tielemans C (1995). Resistance to erythropoietin in iron-overloaded haemodialysis patients can be overcome by ascorbic acid administration. Nephrol. Dial. Transplant. 10 (Suppl 6), 44–47.

Gautier EF, Leduc M, Ladli M, Schulz VP, Lefeévre C, Boussaid I, Fontenay M, Lacombe C, Verdier F, Guillonneau F, et al. (2020). Comprehensive proteomic analysis of murine terminal erythroid differentiation. Blood Adv. 4, 1464–1477. [PubMed: 32282884]

Goasguen JE, Bennett JM, Bain BJ, Brunning R, Vallespi MT, Tomonaga M, Zini G, and Renault A; The International Working Group on Morphology of MDS (2018). Dyserythropoiesis in the diagnosis of the myelodysplastic syndromes and other myeloid neoplasms: problem areas. Br. J. Haematol. 182, 526–533. [PubMed: 29917221]

Grassian AR, Parker SJ, Davidson SM, Divakaruni AS, Green CR, Zhang X, Slocum KL, Pu M, Lin F, Vickers C, et al. (2014). IDH1 mutations alter citric acid cycle metabolism and increase dependence on oxidative mitochondrial metabolism. Cancer Res. 74, 3317–3331. [PubMed: 24755473]

Guo S, Jiang X, Wang Y, Chen L, Li H, Li X, and Jia Y (2017). The protective role of TET2 in erythroid iron homeostasis against oxidative stress and erythropoiesis. Cell. Signal. 38, 106–115. [PubMed: 28697999]

Hata R, and Senoo H (1989). L-ascorbic acid 2-phosphate stimulates collagen accumulation, cell proliferation, and formation of a three-dimensional tissuelike substance by skin fibroblasts. J. Cell. Physiol. 138, 8–16. [PubMed: 2910890]

Held MA, Greenfest-Allen E, Jachimowicz E, Stoeckert CJ, Stokes MP, Wood AW, and Wojchowski DM (2020). Phospho-proteomic discovery of novel EPO signal transducers including thioredoxin-interacting protein as a mediator of EPO-dependent human erythropoiesis. Exp. Hematol. 84, 29–44. [PubMed: 32259549]

Helgerson AL, and Carruthers A (1987). Equilibrium ligand binding to the human erythrocyte sugar transporter. Evidence for two sugar-binding sites per carrier. J. Biol. Chem. 262, 5464–5475. [PubMed: 3571218]

Hu J, Liu J, Xue F, Halverson G, Reid M, Guo A, Chen L, Raza A, Galili N, Jaffray J, et al. (2013). Isolation and functional characterization of human erythroblasts at distinct stages: implications for understanding of normal and disordered erythropoiesis in vivo. Blood 121, 3246–3253. [PubMed: 23422750]

Huang NJ, Lin YC, Lin CY, Pishesha N, Lewis CA, Freinkman E, Farquharson C, Millá n JL, and Lodish H (2018). Enhanced phosphocholine metabolism is essential for terminal erythropoiesis. Blood 131, 2955–2966. [PubMed: 29712634]

Hyde BB, Liesa M, Elorza AA, Qiu W, Haigh SE, Richey L, Mikkola HK, Schlaeger TM, and Shirihai OS (2012). The mitochondrial transporter ABC-me (ABCB10), a downstream target of GATA-1, is essential for erythropoiesis in vivo. Cell Death Differ. 19, 1117–1126. [PubMed: 22240895]

Inoue S, Lemonnier F, and Mak TW (2016). Roles of IDH1/2 and TET2 mutations in myeloid disorders. Int. J. Hematol. 103, 627–633. [PubMed: 26980223]

Iolascon A, D'Agostaro G, Perrotta S, Izzo P, Tavano R, and Miraglia del Giudice B (1996). Congenital dyserythropoietic anemia type II: molecular basis and clinical aspects. Haematologica 81, 543–559. [PubMed: 9009444]

Jang YY, and Sharkis SJ (2007). A low level of reactive oxygen species selects for primitive hematopoietic stem cells that may reside in the low-oxygenic niche. Blood 110, 3056–3063. [PubMed: 17595331]

Johnson RJ, Gaucher EA, Sautin YY, Henderson GN, Angerhofer AJ, and Benner SA (2008). The planetary biology of ascorbate and uric acid and their relationship with the epidemic of obesity and cardiovascular disease. Med. Hypotheses 71, 22–31. [PubMed: 18331782]

Kautz L, and Nemeth E (2014). Molecular liaisons between erythropoiesis and iron metabolism. Blood 124, 479–482. [PubMed: 24876565]

Kc S, Cárcamo JM, and Golde DW (2005). Vitamin C enters mitochondria via facilitative glucose transporter 1 (Glut1) and confers mitochondrial protection against oxidative injury. FASEB J. 19, 1657–1667. [PubMed: 16195374]

Keerthivasan G, Wickrema A, and Crispino JD (2011). Erythroblast enucleation. Stem Cells Int. 2011, 139851. [PubMed: 22007239]

Kim FJ, Manel N, Garrido EN, Valle C, Sitbon M, and Battini JL (2004). HTLV-1 and −2 envelope SU subdomains and critical determinants in receptor binding. Retrovirology 1, 41. [PubMed: 15575958]

Kinet S, Swainson L, Lavanya M, Mongellaz C, Montel-Hagen A, Craveiro M, Manel N, Battini JL, Sitbon M, and Taylor N (2007). Isolated receptor binding domains of HTLV-1 and HTLV-2 envelopes bind Glut-1 on activated CD4+ and CD8+ T cells. Retrovirology 4, 31. [PubMed: 17504522]

Kosmider O, Gelsi-Boyer V, Slama L, Dreyfus F, Beyne-Rauzy O, Quesnel B, Hunault-Berger M, Slama B, Vey N, Lacombe C, et al. (2010). Mutations of IDH1 and IDH2 genes in early

and accelerated phases of myelodysplastic syndromes and MDS/myeloproliferative neoplasms. Leukemia 24, 1094–1096. [PubMed: 20376084]

Kosmider O, Delabesse E, de Mas VM, Cornillet-Lefebvre P, Blanchet O, Delmer A, Recher C, Raynaud S, Bouscary D, Viguié F, et al. ; GOE-LAMS Investigators (2011). TET2 mutations in secondary acute myeloid leukemias: a French retrospective study. Haematologica 96, 1059–1063. [PubMed: 21508122]

Li J, Hale J, Bhagia P, Xue F, Chen L, Jaffray J, Yan H, Lane J, Gallagher PG, Mohandas N, et al. (2014). Isolation and transcriptome analyses of human erythroid progenitors: BFU-E and CFU-E. Blood 124, 3636–3645. [PubMed: 25339359]

Liu J, Xia H, Kim M, Xu L, Li Y, Zhang L, Cai Y, Norberg HV, Zhang T, Furuya T, et al. (2011). Beclin1 controls the levels of p53 by regulating the deubiquitination activity of USP10 and USP13. Cell 147, 223–234. [PubMed: 21962518]

Liu X, Zhang Y, Ni M, Cao H, Signer RAJ, Li D, Li M, Gu Z, Hu Z, Dickerson KE, et al. (2017). Regulation of mitochondrial biogenesis in erythropoiesis by mTORC1-mediated protein translation. Nat. Cell Biol. 19, 626–638. [PubMed: 28504707]

Loisel-Meyer S, Swainson L, Craveiro M, Oburoglu L, Mongellaz C, Costa C, Martinez M, Cosset FL, Battini JL, Herzenberg LA, et al. (2012). Glut1-mediated glucose transport regulates HIV infection. Proc. Natl. Acad. Sci. USA 109, 2549–2554. [PubMed: 22308487]

Ludwig LS, Lareau CA, Bao EL, Nandakumar SK, Muus C, Ulirsch JC, Chowdhary K, Buenrostro JD, Mohandas N, An X, et al. (2019). Transcriptional states and chromatin accessibility underlying human erythropoiesis. Cell Rep. 27, 3228–3240.e7. [PubMed: 31189107]

Luo ST, Zhang DM, Qin Q, Lu L, Luo M, Guo FC, Shi HS, Jiang L, Shao B, Li M, et al. (2017). The promotion of erythropoiesis via the regulation of reactive oxygen species by lactic acid. Sci. Rep. 7, 38105. [PubMed: 28165036]

Manel N, Kim FJ, Kinet S, Taylor N, Sitbon M, and Battini JL (2003). The ubiquitous glucose transporter GLUT-1 is a receptor for HTLV. Cell 115, 449–459. [PubMed: 14622599]

Manning J, Mitchell B, Appadurai DA, Shakya A, Pierce LJ, Wang H, Nganga V, Swanson PC, May JM, Tantin D, and Spangrude GJ (2013). Vitamin C promotes maturation of T-cells. Antioxid. Redox Signal. 19, 2054–2067. [PubMed: 23249337]

Mantel C, Messina-Graham S, and Broxmeyer HE (2010). Upregulation of nascent mitochondrial biogenesis in mouse hematopoietic stem cells parallels upregulation of CD34 and loss of pluripotency: a potential strategy for reducing oxidative risk in stem cells. Cell Cycle 9, 2008–2017. [PubMed: 20495374]

Maryanovich M, Zaltsman Y, Ruggiero A, Goldman A, Shachnai L, Zaidman SL, Porat Z, Golan K, Lapidot T, and Gross A (2015). An MTCH2 pathway repressing mitochondria metabolism regulates haematopoietic stem cell fate. Nat. Commun. 6, 7901. [PubMed: 26219591]

May JM (1998). Ascorbate function and metabolism in the human erythrocyte. Front. Biosci. 3, d1–d10. [PubMed: 9405334]

May JM, Qu Z, and Morrow JD (2001). Mechanisms of ascorbic acid recycling in human erythrocytes. Biochim. Biophys. Acta 1528, 159–166. [PubMed: 11687303]

McNulty AL, Stabler TV, Vail TP, McDaniel GE, and Kraus VB (2005). Dehydroascorbate transport in human chondrocytes is regulated by hypoxia and is a physiologically relevant source of ascorbic acid in the joint. Arthritis Rheum. 52, 2676–2685. [PubMed: 16142743]

Metallo CM, Gameiro PA, Bell EL, Mattaini KR, Yang J, Hiller K, Jewell CM, Johnson ZR, Irvine DJ, Guarente L, et al. (2011). Reductive glutamine metabolism by IDH1 mediates lipogenesis under hypoxia. Nature 481, 380–384. [PubMed: 22101433]

Mingay M, Chaturvedi A, Bilenky M, Cao Q, Jackson L, Hui T, Moksa M, Heravi-Moussavi A, Humphries RK, Heuser M, and Hirst M (2018). Vitamin C-induced epigenomic remodelling in IDH1 mutant acute myeloid leukaemia. Leukemia 32, 11–20. [PubMed: 28663574]

Montel-Hagen A, Blanc L, Boyer-Clavel M, Jacquet C, Vidal M, Sitbon M, and Taylor N (2008a). The Glut1 and Glut4 glucose transporters are differentially expressed during perinatal and postnatal erythropoiesis. Blood 112, 4729–4738. [PubMed: 18796630]

Montel-Hagen A, Kinet S, Manel N, Mongellaz C, Prohaska R, Battini JL, Delaunay J, Sitbon M, and Taylor N (2008b). Erythrocyte Glut1 triggers dehydroascorbic acid uptake in mammals unable to synthesize vitamin C. Cell 132, 1039–1048. [PubMed: 18358815]

Montel-Hagen A, Sitbon M, and Taylor N (2009). Erythroid glucose transporters. Curr. Opin. Hematol. 16, 165–172. [PubMed: 19346941]

Moras M, Lefevre SD, and Ostuni MA (2017). From erythroblasts to mature red blood cells: organelle clearance in mammals. Front. Physiol. 8, 1076. [PubMed: 29311991]

Mueckler M (1994). Facilitative glucose transporters. Eur. J. Biochem. 219, 713–725. [PubMed: 8112322]

Murphy MP (2009). How mitochondria produce reactive oxygen species. Biochem. J. 417, 1–13. [PubMed: 19061483]

Oburoglu L, Tardito S, Fritz V, de Barros SC, Merida P, Craveiro M, Mamede J, Cretenet G, Mongellaz C, An X, et al. (2014). Glucose and glutamine metabolism regulate human hematopoietic stem cell lineage specification. Cell Stem Cell 15, 169–184. [PubMed: 24953180]

Oburoglu L, Romano M, Taylor N, and Kinet S (2016). Metabolic regulation of hematopoietic stem cell commitment and erythroid differentiation. Curr. Opin. Hematol. 23, 198–205. [PubMed: 26871253]

Padayatty SJ, and Levine M (2016). Vitamin C: the known and the unknown and Goldilocks. Oral Dis. 22, 463–493. [PubMed: 26808119]

Pauling L (1970). Evolution and the need for ascorbic acid. Proc. Natl. Acad. Sci. USA 67, 1643–1648. [PubMed: 5275366]

Qian P, He XC, Paulson A, Li Z, Tao F, Perry JM, Guo F, Zhao M, Zhi L, Venkatraman A, et al. (2016). The Dlk1-Gtl2 locus preserves LT-HSC function by inhibiting the PI3K-mTOR pathway to restrict mitochondrial metabolism. Cell Stem Cell 18, 214–228. [PubMed: 26627594]

Qu X, Zhang S, Wang S, Wang Y, Li W, Huang Y, Zhao H, Wu X, An C, Guo X, et al. (2018). TET2 deficiency leads to stem cell factor-dependent clonal expansion of dysfunctional erythroid progenitors. Blood 132, 2406–2417. [PubMed: 30254129]

Robb EL, Gawel JM, Aksentijević D, Cochemé HM, Stewart TS, Shchepinova MM, Qiang H, Prime TA, Bright TP, James AM, et al. (2015). Selective superoxide generation within mitochondria by the targeted redox cycler MitoParaquat. Free Radic. Biol. Med. 89, 883–894. [PubMed: 26454075]

Rumsey SC, Kwon O, Xu GW, Burant CF, Simpson I, and Levine M (1997). Glucose transporter isoforms GLUT1 and GLUT3 transport dehydroascorbic acid. J. Biol. Chem. 272, 18982–18989. [PubMed: 9228080]

Rumsey SC, Daruwala R, Al-Hasani H, Zarnowski MJ, Simpson IA, and Levine M (2000). Dehydroascorbic acid transport by GLUT4 in Xenopus oocytes and isolated rat adipocytes. J. Biol. Chem. 275, 28246–28253. [PubMed: 10862609]

Savini I, Rossi A, Pierro C, Avigliano L, and Catani MV (2008). SVCT1 and SVCT2: key proteins for vitamin C uptake. Amino Acids 34, 347–355. [PubMed: 17541511]

Schulz VP, Yan H, Lezon-Geyda K, An X, Hale J, Hillyer CD, Mohandas N, and Gallagher PG (2019). A unique epigenomic landscape defines human erythropoiesis. Cell Rep. 28, 2996–3009.e7. [PubMed: 31509757]

Seibert E, Richter A, Kuhlmann MK, Wang S, Levin NW, Kotanko P, and Handelman GJ (2017). Plasma vitamin C levels in ESRD patients and occurrence of hypochromic erythrocytes. Hemodial. Int. 21, 250–255. [PubMed: 27619554]

Shenoy N, Creagan E, Witzig T, and Levine M (2018). Ascorbic acid in cancer treatment: let the phoenix fly. Cancer Cell 34, 700–706. [PubMed: 30174242]

Sirover WD, Siddiqui AA, and Benz RL (2008). Beneficial hematologic effects of daily oral ascorbic acid therapy in ESRD patients with anemia and abnormal iron homeostasis: a preliminary study. Ren. Fail. 30, 884–889. [PubMed: 18925528]

Starkov AA, Fiskum G, Chinopoulos C, Lorenzo BJ, Browne SE, Patel MS, and Beal MF (2004). Mitochondrial alpha-ketoglutarate dehydrogenase complex generates reactive oxygen species. J. Neurosci. 24, 7779–7788. [PubMed: 15356189]

Stone I (1979). Eight decades of scurvy. Australas. Nurses J. 8, 28–30.

Suda T, Takubo K, and Semenza GL (2011). Metabolic regulation of hematopoietic stem cells in the hypoxic niche. Cell Stem Cell 9, 298–310. [PubMed: 21982230]

Swainson L, Kinet S, Manel N, Battini JL, Sitbon M, and Taylor N (2005). Glucose transporter 1 expression identifies a population of cycling CD4+ CD8+ human thymocytes with high CXCR4-induced chemotaxis. Proc. Natl. Acad. Sci. USA 102, 12867–12872. [PubMed: 16126902]

Takamizawa S, Maehata Y, Imai K, Senoo H, Sato S, and Hata R (2004). Effects of ascorbic acid and ascorbic acid 2-phosphate, a long-acting vitamin C derivative, on the proliferation and differentiation of human osteoblast-like cells. Cell Biol. Int. 28, 255–265. [PubMed: 15109981]

Takubo K, Nagamatsu G, Kobayashi CI, Nakamura-Ishizu A, Kobayashi H, Ikeda E, Goda N, Rahimi Y, Johnson RS, Soga T, et al. (2013). Regulation of glycolysis by Pdk functions as a metabolic checkpoint for cell cycle quiescence in hematopoietic stem cells. Cell Stem Cell 12, 49–61. [PubMed: 23290136]

Tan DQ, and Suda T (2018). Reactive oxygen species and mitochondrial homeostasis as regulators of stem cell fate and function. Antioxid. Redox Signal. 29, 149–168. [PubMed: 28708000]

TeSlaa T, Chaikovsky AC, Lipchina I, Escobar SL, Hochedlinger K, Huang J, Graeber TG, Braas D, and Teitell MA (2016). α-Ketoglutarate accelerates the initial differentiation of primed human pluripotent stem cells. Cell Metab. 24, 485–493. [PubMed: 27476976]

Tischler J, Gruhn WH, Reid J, Allgeyer E, Buettner F, Marr C, Theis F, Simons BD, Wernisch L, and Surani MA (2019). Metabolic regulation of pluripotency and germ cell fate through α-ketoglutarate. EMBO J. 38, 38.

Tretter L, and Adam-Vizi V (2004). Generation of reactive oxygen species in the reaction catalyzed by alpha-ketoglutarate dehydrogenase. J. Neurosci. 24, 7771–7778. [PubMed: 15356188]

Tsukaguchi H, Tokui T, Mackenzie B, Berger UV, Chen XZ, Wang Y, Brubaker RF, and Hediger MA (1999). A family of mammalian Na+-dependent L-ascorbic acid transporters. Nature 399, 70–75. [PubMed: 10331392]

Vande Voorde J, Ackermann T, Pfetzer N, Sumpton D, Mackay G, Kalna G, Nixon C, Blyth K, Gottlieb E, and Tardito S (2019). Improving the metabolic fidelity of cancer models with a physiological cell culture medium. Sci. Adv. 5, eaau7314. [PubMed: 30613774]

Vannini N, Girotra M, Naveiras O, Nikitin G, Campos V, Giger S, Roch A, Auwerx J, and Lutolf MP (2016). Specification of haematopoietic stem cell fate via modulation of mitochondrial activity. Nat. Commun. 7, 13125. [PubMed: 27731316]

Vardhana SA, Arnold PK, Rosen BP, Chen Y, Carey BW, Huangfu D, Carmona Fontaine C, Thompson CB, and Finley LWS (2019). Glutamine independence is a selectable feature of pluripotent stem cells. Nat. Metab. 1, 676–687. [PubMed: 31511848]

Vera JC, Rivas CI, Fischbarg J, and Golde DW (1993). Mammalian facilitative hexose transporters mediate the transport of dehydroascorbic acid. Nature 364, 79–82. [PubMed: 8316303]

Wang N, Wang F, Shan N, Sui X, and Xu H (2017). IDH1 mutation is an independent inferior prognostic indicator for patients with myelodysplastic syndromes. Acta Haematol. 138, 143–151. [PubMed: 28873367]

Wilson JX (2005). Regulation of vitamin C transport. Annu. Rev. Nutr. 25, 105–125. [PubMed: 16011461]

Xiao M, Yang H, Xu W, Ma S, Lin H, Zhu H, Liu L, Liu Y, Yang C, Xu Y, et al. (2012). Inhibition of α-KG-dependent histone and DNA demethylases by fumarate and succinate that are accumulated in mutations of FH and SDH tumor suppressors. Genes Dev. 26, 1326–1338. [PubMed: 22677546]

Xu P, Palmer LE, Lechauve C, Zhao G, Yao Y, Luan J, Vourekas A, Tan H, Peng J, Schuetz JD, et al. (2019). Regulation of gene expression by miR-144/451 during mouse erythropoiesis. Blood 133, 2518–2528. [PubMed: 30971389]

Yan H, Wang Y, Qu X, Li J, Hale J, Huang Y, An C, Papoin J, Guo X, Chen L, et al. (2017). Distinct roles for TET family proteins in regulating human erythropoiesis. Blood 129, 2002–2012. [PubMed: 28167661]

Yan H, Hale J, Jaffray J, Li J, Wang Y, Huang Y, An X, Hillyer C, Wang N, Kinet S, et al. (2018). Developmental differences between neonatal and adult human erythropoiesis. Am. J. Hematol. 93, 494–503. [PubMed: 29274096]

Yu WM, Liu X, Shen J, Jovanovic O, Pohl EE, Gerson SL, Finkel T, Broxmeyer HE, and Qu CK (2013). Metabolic regulation by the mitochondrial phosphatase PTPMT1 is required for hematopoietic stem cell differentiation. Cell Stem Cell 12, 62–74. [PubMed: 23290137]

Yun J, Mullarky E, Lu C, Bosch KN, Kavalier A, Rivera K, Roper J, Chio II, Giannopoulou EG, Rago C, et al. (2015). Vitamin C selectively kills KRAS and BRAF mutant colorectal cancer cells by targeting GAPDH. Science 350, 1391–1396. [PubMed: 26541605]

Zhang ZZ, Lee EE, Sudderth J, Yue Y, Zia A, Glass D, Deberardinis RJ, and Wang RC (2016). Glutathione depletion, pentose phosphate pathway activation, and hemolysis in erythrocytes protecting cancer cells from vitamin C-induced oxidative stress. J. Biol. Chem. 291, 22861–22867. [PubMed: 27660392]

Zhao B, Mei Y, Yang J, and Ji P (2016). Erythropoietin-regulated oxidative stress negatively affects enucleation during terminal erythropoiesis. Exp. Hematol. 44, 975–981. [PubMed: 27364565]

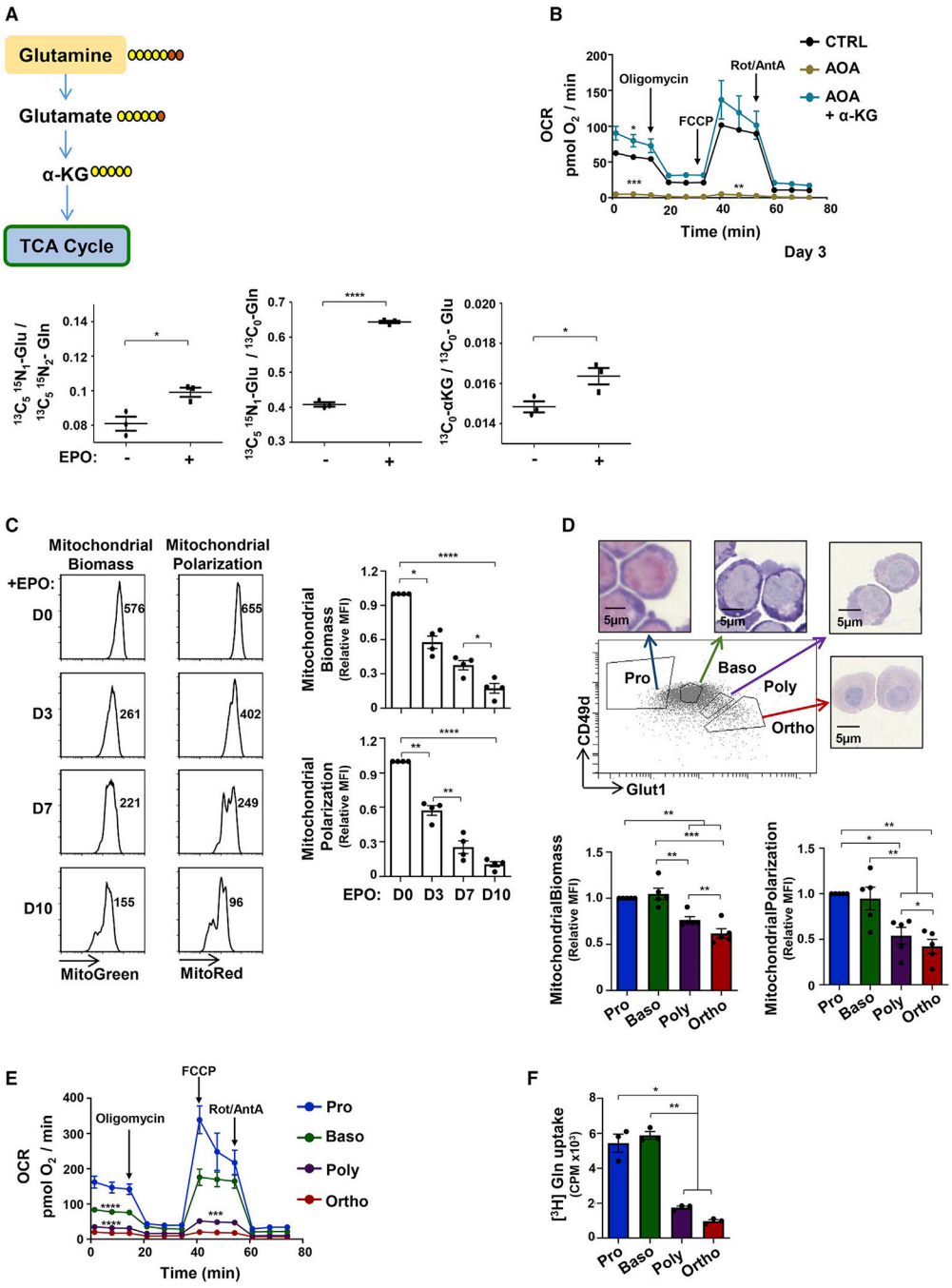

Figure 1. Early erythropoiesis results in increased metabolism followed by decreased mitochondrial activity during terminal erythroid differentiation

(A) Schematic representation of glutamine conversion to α-ketoglutarate (αKG), showing the metabolism of [$^{13}C_5$ $^{15}N_2$] heavy-labeled glutamine (Gln) carbons (yellow) and nitrogens (orange; top). Peak area ratios of heavy atoms from [$^{13}C_5$ $^{15}N_2$]Gln into glutamate ([$^{13}C_5$ $^{15}N_1$]Glu), the relative level of [$^{13}C_5$ $^{15}N_1$]Glu, and the portion of [$^{13}C_5$]αKG at day 4 of differentiation in the absence or presence of rEPO are shown (±SEM). Horizontal lines represent mean levels. Each dot represents an individual technical replicate, representative of one of two independent experiments.

(B) Oxygen consumption rates (OCRs), a measure of OXPHOS, were monitored by sequential injection of oligomycin, FCCP, and rotenone/antimycin A (Rot/AntA) as indicated. Mean basal oxygen consumption, maximal consumption following FCCP, and minimal levels following inhibition of the electron transport chain (ETC) Rot/AntA (bottom panel) are presented at day 3 of erythroid differentiation in control conditions (CTRL), in the presence of the AOA transaminase inhibitor (1 mM) or AOA + αKG (3.5mM). Means ± SEM are presented (n = 3).

(C) Mitochondrial biomass and polarization were evaluated by MitoTracker Green and MitoTracker Red staining, respectively, at days 0, 3, 7, and 10 of differentiation (n = 4).

(D) Pro-erythroblasts (Pro) and basophilic (Baso), polychromatic (Poly), and orthochromatic (Ortho) erythroblasts were sorted as a function of their GLUT1/CD49d profile (top panel). H&E staining of sorted erythroblasts is shown. Mitochondrial biomass and polarization were evaluated as in (C), and means ± SEM are presented (n = 5).

(E) OCR was monitored 15 h post-sorting and means ± SEM are presented (n = 6).

(F) Glutamine uptake was monitored 18 h following sorting using L-[3,4-^{3}H (N)]glutamine (0.5 μCi) for 10 min at room temperature (RT). Uptake is expressed as mean counts per minute (CPM) for triplicate samples ± SEM.

Statistical significance was determined by a one-way ANOVA with Tukey's post hoc test (*p < 0.05; **p < 0.01; ***p < 0.001; ****p < 0.0001).

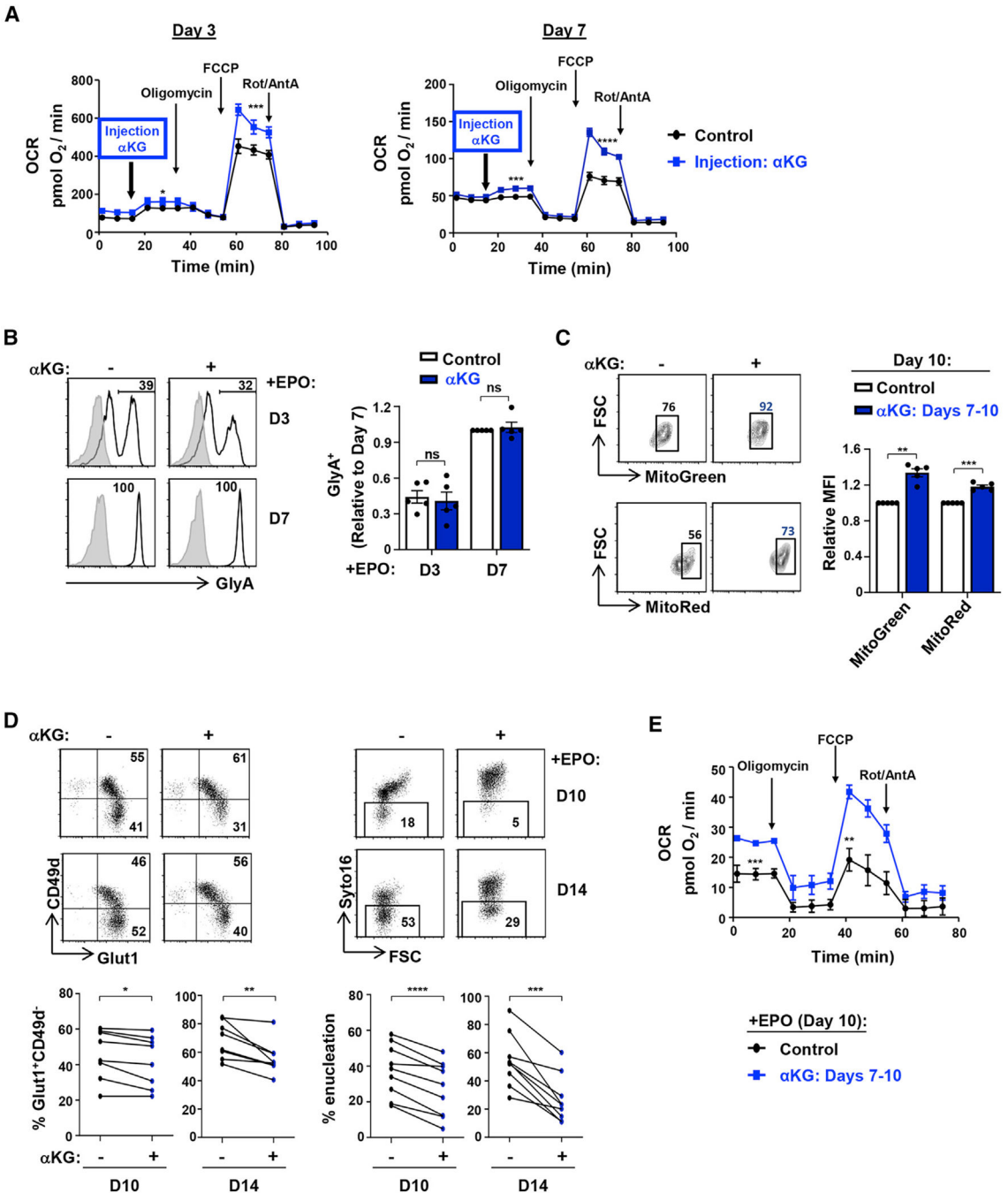

Figure 2. αKG increases mitochondrial function while significantly inhibiting terminal erythroid differentiation and enucleation

(A) CD34$^+$ HSPCs were differentiated with EPO, and OXPHOS was evaluated at days 3 (left) and 7 (right) directly following injection of cell-permeable αKG (3.5 mM, blue line) into the Seahorse analyzer. Mean OCR ± SEM are presented for the indicated conditions (n = 5–6 per time point).

(B) Progenitors were stimulated with rEPO in the absence (−) or presence (+) of αKG. Expression of GlyA was monitored at days 3 and 7, and representative histograms (left) are shown (gray histograms, isotype controls; black lines, specific staining). Mean levels of

GlyA$^+$ cells were quantified in the different conditions (right), with levels at day 7 arbitrarily set at 1 (means ± SEM of five independent experiments; ns, nonsignificant).

(C) Mitochondrial biomass and mitochondrial membrane potential (MMP) were monitored following erythroid differentiation in the absence (−) or presence (+) of αKG (between days 7 and 10). Representative dot plots showing the percentages of cells with high mitochondrial biomass and MMP at day 10 are presented (left). Mean biomass and MMP (±SEM) are presented (right; n = 5).

(D) CD49d/Glut1 profiles of GlyA$^+$ erythroblasts differentiated in the absence or presence of αKG (starting at day 7) were monitored at days 10 and 14 of differentiation, and representative dot plots are shown (top left). Percentages of Glut1$^+$CD49d$^-$ orthochromatic erythroblasts are shown for eight individual donors (bottom left). Erythroblast enucleation was evaluated as a function of Syto16 nucleic acid staining, and representative dot plots indicating the percentages of Syto16$^-$ enucleated cells are presented (top right). Percentage enucleation in nine individual donors is presented (bottom right).

(E) OCR was evaluated on day 10 erythroid progenitors in control conditions (black line) and following addition of αKG at day 7 (blue line). Mean levels ± SEM are presented (n = 5–6).

ns, nonsignificant; *p < 0.05; **p < 0.01; ***p < 0.001; ****p < 0.0001.

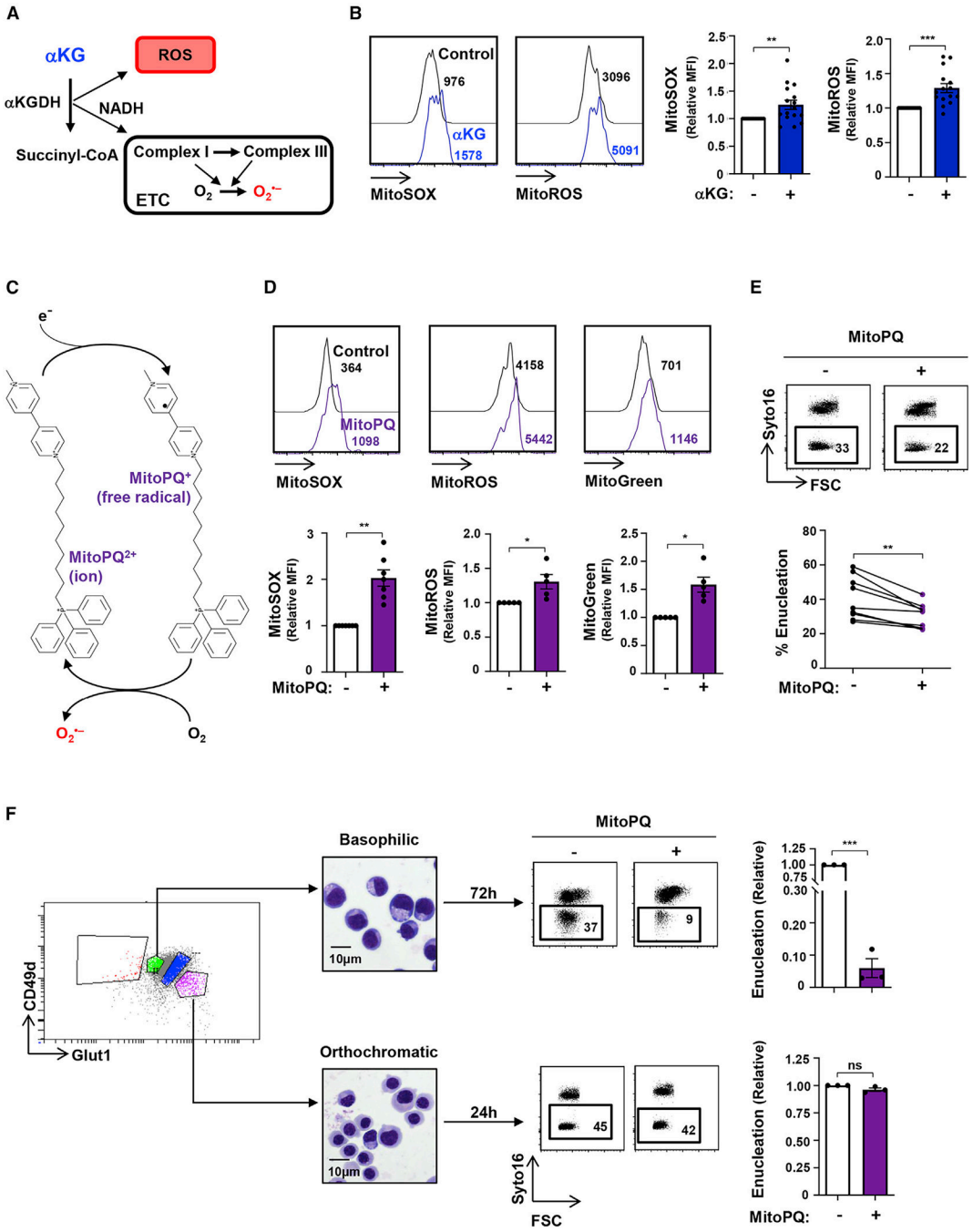

Figure 3. Mitochondrial superoxide production impedes erythroid enucleation

(A) Schematic of the generation of mitochondrial reactive oxygen species (ROS) via the conversion of aKG to succinate, of which superoxide is a major source.

(B) The impact of αKG (3.5 mM) on mitochondrial superoxide and mitochondrial ROS production in erythroblasts was evaluated at day 10 of erythroid differentiation as a function of MitoSOX and MitoROS, respectively. Representative histograms are shown (left). Staining in the presence of αKG was normalized to control conditions, and relative median fluorescence intensities (MFIs) are presented (n = 15–16, right).

(C) Schematic of MitoParaquat (MitoPQ) cycling within the mitochondria; mitoPQ^{2+} is reduced to the radical monocation at the flavin site of complex I, and the monocation then reacts with O_2 to generate superoxide (O_2^-) (Robb et al., 2015).
(D) Differentiating erythroblasts were treated with MitoPQ (50 μM) at day 7 of differentiation, and representative histograms of mitochondrial superoxide, ROS, and biomass at day 10 are presented (top). MFIs are presented relative to control conditions (n = 5–6, bottom).
(E) The impact of MitoPQ on enucleation was evaluated at day 10 by Syto16 staining, and representative dot plots are presented (top). Percent enucleation in nine independent experiments is shown (bottom).
(F) The impact of MitoPQ on early basophilic erythroblasts as compared to late orthochromatic erythroblasts was determined by FACS sorting erythroblast populations as a function of their GLUT1/CD49d profiles (left), and representative cytospins of the sorted subsets are shown (middle). Early basophilic and late orthochromatic subsets were then cultured for 72 h or 24 h, respectively, in the absence (−) or presence (+) of MitoPQ, and enucleation was evaluated (right). Enucleation was quantified relative to control conditions (n = 3).
ns, nonsignificant; *p < 0.05; **p < 0.01; ***p < 0.001.

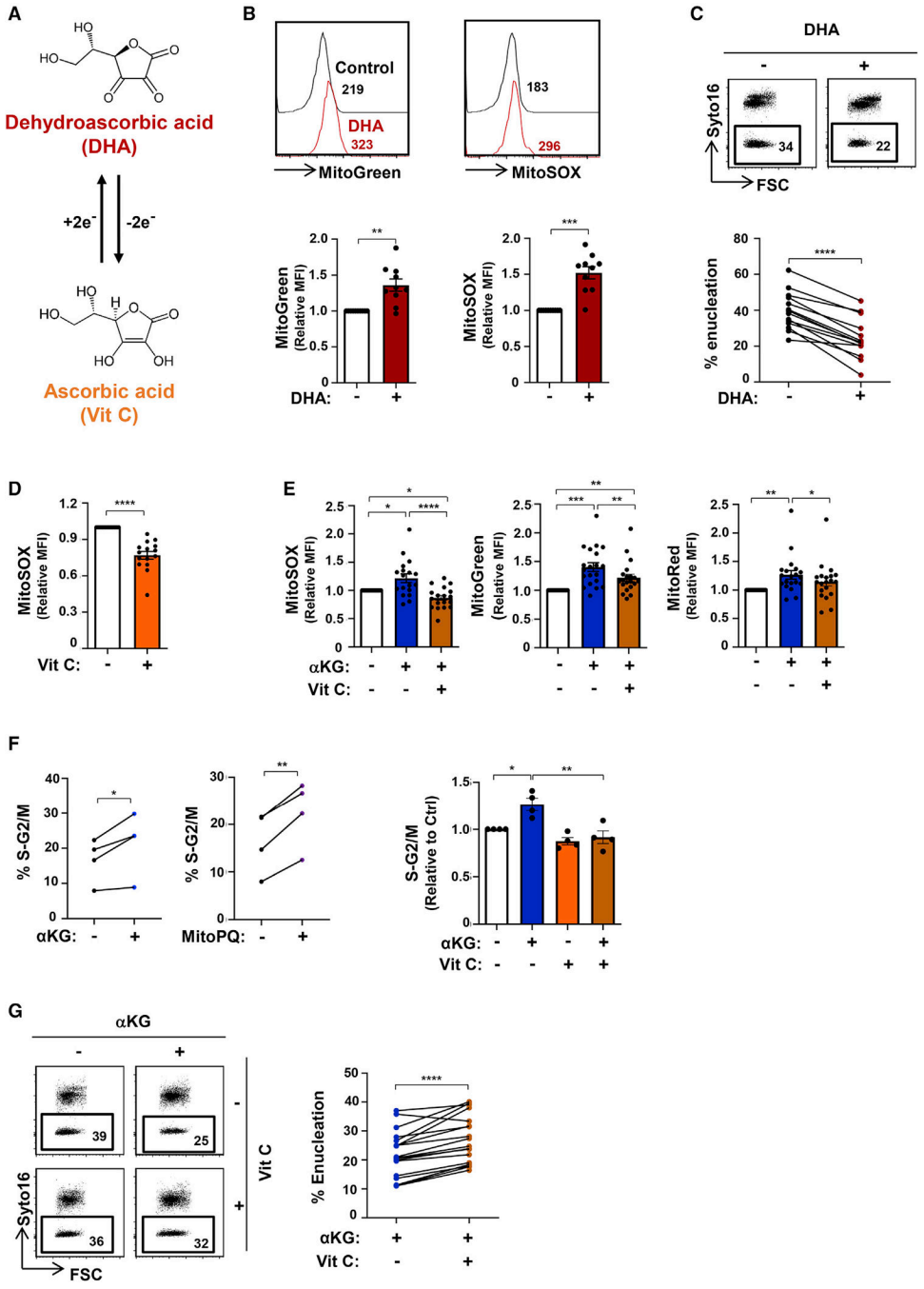

Figure 4. Antagonistic roles of dehydroascorbic acid and vitamin C on mitochondrial oxidative stress and erythroblast enucleation

(A) Schematic of the interconversion between dehydroascorbic acid (DHA) and ascorbic acid (vitamin C) via a two-electron reduction/oxidation process, respectively.

(B) The impact of DHA (1 mM) on mitochondrial superoxide production and biomass in late erythroblasts was evaluated between days 7 and 10 after EPO induction, and representative histograms of MitoGreen and MitoSOX staining, respectively, are shown (top). Quantification relative to control conditions is shown (n = 10, bottom).

(C) Enucleation was evaluated at day 10 after EPO induction in the absence (−) or presence (+) of DHA (days 7–10), and representative dot plots are shown (top). Percent enucleation in 14 independent experiments is presented (bottom).
(D) The impact of the stable L-ascorbic acid (AA) 2-phosphate derivative of vitamin C (100 μM) was evaluated on mitochondrial superoxide generation (days 7–10), and MFIs were quantified relative to control conditions (n = 15, bottom).
(E) The impact of vitamin C on αKG-mediated increases in MitoSOX, MitoGreen, and MitoRed staining was evaluated by flow cytometry, and relative MFIs are presented (n = 18–20).
(F) The percentages of cells in S-G2/M of the cell cycle were evaluated in the indicated conditions by phosphatidylinositol (PI) staining (n = 4, left). The percentages of erythroid progenitors in S-G2/M were evaluated relative to control conditions, and means ± SEM are presented (right).
(G) Enucleation was evaluated in the presence or absence of vitamin C and αKG. Representative histograms (left) as well as changes in percent enucleation are presented (n = 18, right).
*p < 0.05; **p < 0.01; ***p < 0.001;****p < 0.0001.

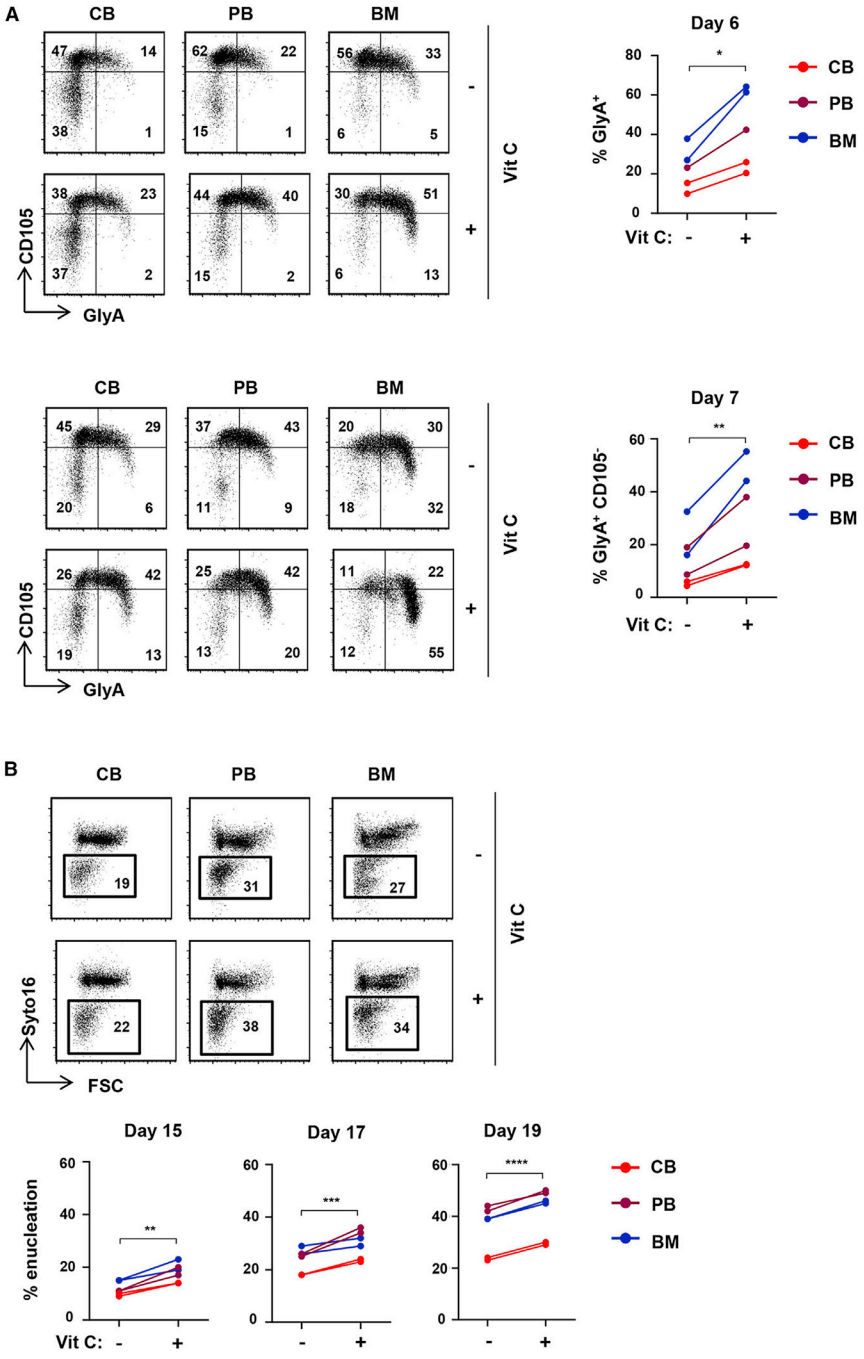

Figure 5. Vitamin C promotes erythroid commitment of EPO-stimulated progenitors from CB, BM, and PB and significantly accelerates erythroid maturation

(A) $CD34^+$ HSPCs were isolated from CB, PB, and BM. Progenitors were differentiated with EPO in the absence or presence of vitamin C (100 μM) and erythropoiesis monitored as a function of CD105/GlyA profiles. Representative profiles at days 6 (top left) and 7 (bottom left) of differentiation are presented. Quantification of $GlyA^+$ cells at day 6 (n = 5, top right) and $GlyA^+CD105^-$ cells at day 7 (n = 5, bottom right) is presented.

(B) The impact of vitamin C on enucleation was evaluated in CB, PB, and BM HSPCs, and representative plots at day 17 are presented (top). Quantification of enucleation at days 15, 17, and 19 is presented (n = 6, bottom).
*p < 0.05; **p < 0.01; ***p < 0.001; ****p < 0.0001.

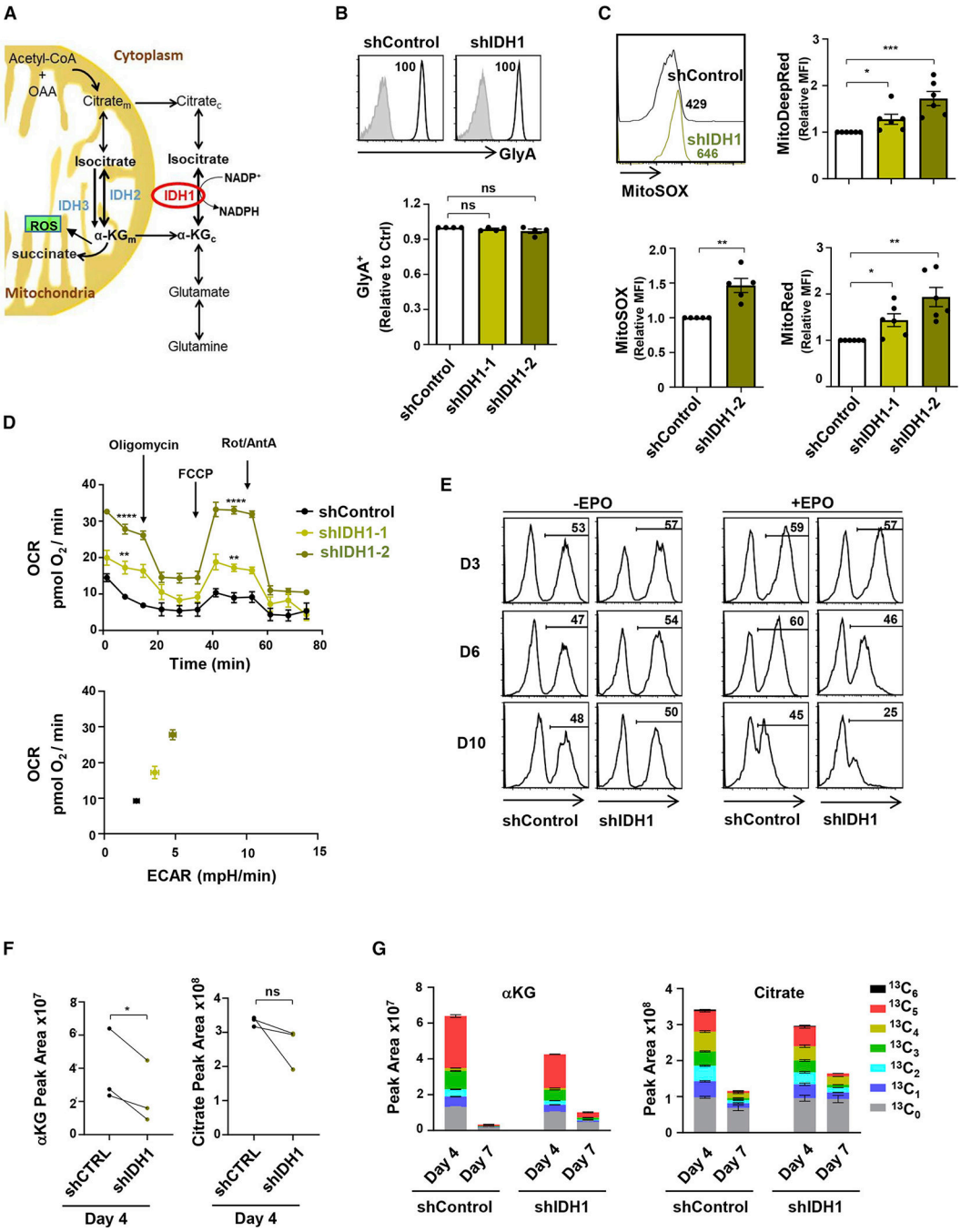

Figure 6. IDH activity regulates mitochondrial superoxide production and OXPHOS in differentiation erythroblasts

(A) Schematic representation of the catalytic reactions regulating glutamine catabolism. Glutamine is interconverted to glutamate and cytosolic αKG (αKG$_c$). Isocitrate dehydrogenase 1 (IDH1), a cytosolic enzyme, catalyzes the production of isocitrate from αKG, promoting both forward and reverse reactions. Conversion of mitochondrial αKG (αKG$_m$) to succinate results in the generation of ROS.

(B) The expression of GlyA was monitored in shControl- and shIDH1-transduced cells at day 7 day of differentiation, and representative histograms (gray, isotype control; black,

specific staining) are shown (top). GlyA expression in cells transduced with one of two different shIDH1 clones (shIDH1–1 and shIDH1–2) was evaluated, and relative levels are presented (n = 4, bottom).

(C) The impact of IDH1 downregulation on MitoSOX was evaluated at day 10. Representative histograms (top left) and quantification of relative MFIs (n = 5) are presented (bottom left). MitoTracker Deep Red (top right) and MitoTracker Red (bottom right) staining in shIDH1-transduced erythroblasts relative to control conditions, are presented (n = 6).

(D) OCR was determined in FACS-sorted shControl- as well as shIDH1-transduced erythroblasts at day 10 of differentiation as indicated (n = 6, top). An OCR/extracellular acidification rate (ECAR) energy map is presented (bottom).

(E) The evolution of shControl- and sh-IDH1-transduced progenitors was monitored as a function of GFP expression at days 3, 6, and 10 of differentiation in the absence (−) or presence (+) of EPO (n = 3).

(F) Total levels of αKG and citrate were evaluated by high-performance liquid chromatography-mass spectrometry (HPLC-MS) at day 4 of erythroid differentiation in shControl- and shIDH1-transduced progenitors, and mean levels are shown (n = 3 independent experiments, with statistical difference evaluated by a one-tailed t test).

(G) The isotopologues of αKG and citrate derived from [$^{13}C_5$ $^{15}N_2$]Gln are presented from one experiment with three replicates for day 4 and two replicates for day 7.

ns, not significant; *p < 0.05; **p < 0.01; ***p < 0.001; ****p < 0.0001.

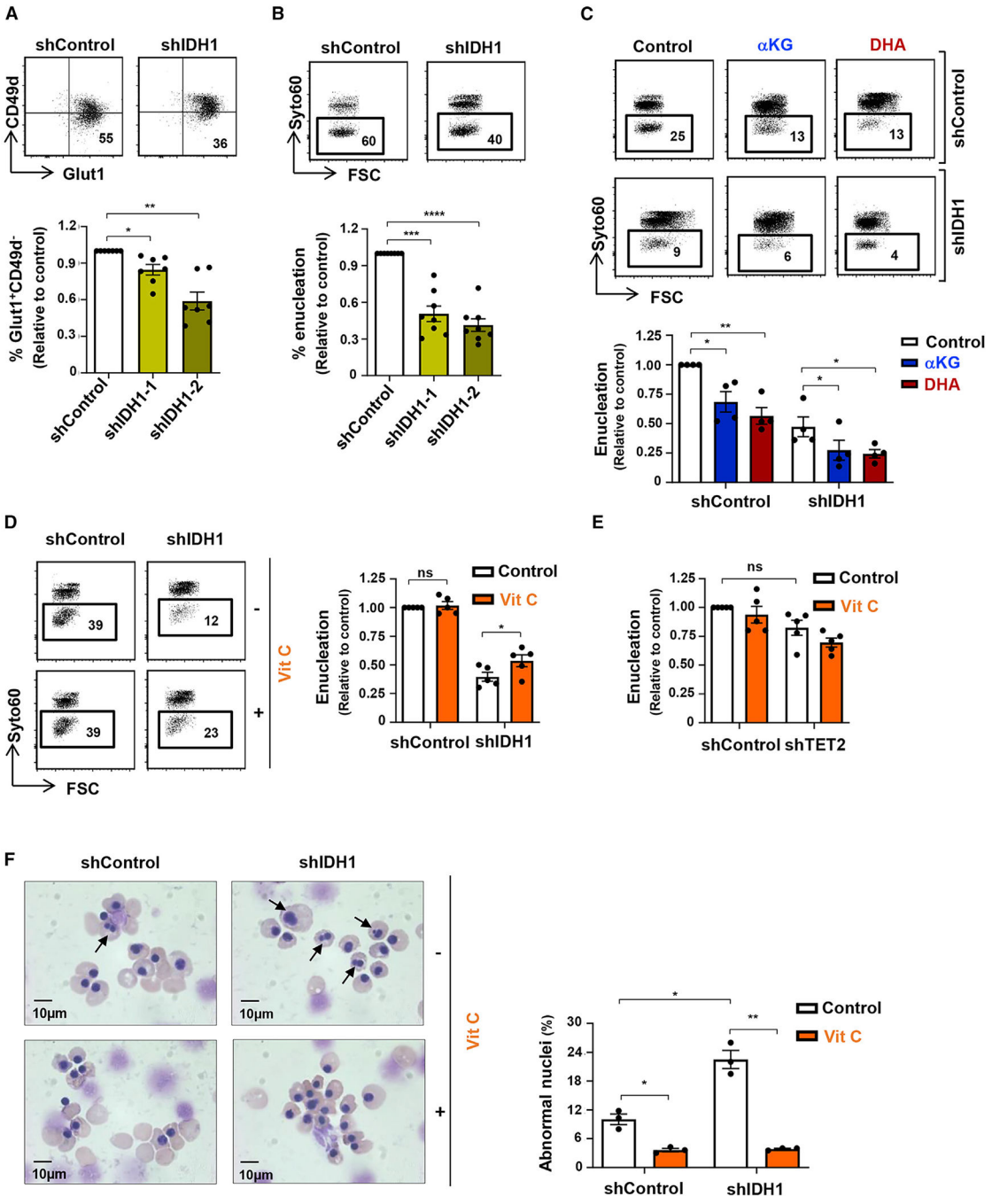

Figure 7. Vitamin C rescues dyserythropoiesis due to IDH1 downregulation

(A) Late-stage erythroblast differentiation was monitored as a GLUT1^{+}CD49d^{-} phenotype, and representative dot plots are presented (top). The percentages of GLUT1^{+}CD49d^{-} erythroblasts were evaluated following transduction with shIDH1–1 or shIDH1–2 vectors, and mean levels ± SEM relative to control cells are presented (n = 7, bottom).

(B) Enucleation of shControl- and shIDH1-transduced erythroblasts was assessed on GFP+ cells at day 14, and representative histograms are presented (top). Enucleation levels, relative to control cells, were quantified (n = 8, bottom).

(C) The impact of αKG and DHA on erythroblast enucleation following IDH1 knockdown was evaluated between days 7 and 10, and representative histograms are presented (top). Enucleation relative to control conditions was quantified (n = 4, bottom).
(D) The impact of vitamin C on enucleation of control and IDH1-downregulated erythroblasts was evaluated between days 7 and 10. Representative histograms (top) and quantifications (bottom) are presented (n = 5). Changes in mitochondrial superoxide were evaluated by MitoSOX staining, and MFIs are presented (n = 4).
(E) TET2 was downregulated in erythroid progenitors by shTET2 lentivirus (day 4), and enucleation was monitored at day 10 in the presence or absence of vitamin C. Means ± SEM are presented (n = 5, one-way ANOVA with Tukey's post hoc test).
(F) Nuclear morphology of orthochromatic erythroblasts differentiated from shControl- and shIDH1-transduced progenitors in the absence or presence of vitamin C was monitored. Representative cytospins are shown (left), and the quantification of orthochromatic erythroblasts with abnormal nuclei was determined by counting 500–1,000 cells (n = 3, right).
ns, not significant; *p < 0.05; **p < 0.01; ***p < 0.001; ****p < 0.0001.

KEY RESOURCES TABLE

REAGENT or RESOURCE	SOURCE	IDENTIFIER
Antibodies		
Anti-hCD11b-PE (clone Bearl)	Beckman Coulter	Cat#IM2581U; RRID: AB_131334
Anti-hCD13-PC7 (clone Immuno103.44)	Beckman Coulter	Cat#A46528
Anti-hCD33 (clone D3HL60.251)	Beckman Coulter	Cat#A07775
Anti-hCD34-FITC (clone 581)	Becton Dickinson	Cat#55582;RRID:AB_396150
Anti-hCD34-APC (clone 581)	Becton Dickinson	Cat#555824; RRID:AB_398614
Anti-hCD34-PE (clone 81)	Beckman Coulter	Cat#A07776
Anti-hCD36-APC (clone FA6.152)	Beckman Coulter	Cat#A87786
Anti-hCD36-FITC (clone FA6.152)	Beckman Coulter	Cat#B49201; RRID:AB_2848117
Anti-hCD36-PB (clone FA6.152)	Beckman Coulter	Cat#B43302
Anti-hCD49d-APC (clone HP2/1)	Beckman Coulter	Cat#B01682
Anti-hCD71-APC (clone MA-A712)	Becton Dickinson	Cat#551374; RRID:AB_398500
Anti-hCD71-APC-AF750 (clone MA-A712)	Beckman Coulter	Cat#A89313; RRID:AB_2800452
Anti-hCD105- PECF594 (clone 266)	Becton Dickinson	Cat#562380; RRID:AB_11154054
Anti-hGlyA-PC7 (clone 11E4B-7-6)	Beckman Coulter	Cat#A71564; RRID:AB_2800449
Anti-hGlyA-APC (clone GA-R2 (HIR2))	eBioscience/ThermoFisher	Cat#17-9987-42; RRID:AB_2043823
Anti-hGlyA- BV421 (clone GA-R2 (HIR2))	Becton Dickinson	Cat#562938
Anti-hIL3R-PC7 (clone 6H6)	eBioscience/ThermoFisher	Cat#25-1239-42; RRID:AB_1257136
Goat anti-Rabbit IgG Alexa Fluor 405	Molecular Probes/ThermoFisher	Cat#A-31556; RRID:AB_221605
GLUT1 RBD-GFP	Metafora Biosystems	Cat#GLUT1_G100
GLUT1 RBD-rFc	Metafora Biosystems	Cat#GLUT1_R100
Bacterial and virus strains		
Top 10 Compotent cells	ThermoFisher	Cat#C404010
Biological samples		
Human umbilical cord blood	Unite De Therapie Cellulaire de Montpellier	N/A
Human peripheral blood	New York Blood Center	N/A
Human bone marrow	Northwell Health	N/A
Chemicals, peptides, and recombinant proteins		
2-Phospho-L-ascorbic acid	Sigma-Aldrich	Cat#A8960
tetramethylchromane-2-carboxylic acid (TROLOX)	Sigma-Aldrich	Cat#238813
N-Acetylcysteine	Sigma-Aldrich	Cat#A9165
Ascorbate Oxidase from Cucurbita sp.	Sigma-Aldrich	Cat#A0157
L-Ascorbic acid	Sigma-Aldrich	Cat#A92902
O-(Carboxymethyl)hydroxylamine hemihydrochloride (AOA)	Sigma-Aldrich	Cat#C13408
Diethylsuccinate	Sigma-Aldrich	Cat#112402
Dimethyl α-ketoglutarate	Sigma-Aldrich	Cat#349631

REAGENT or RESOURCE	SOURCE	IDENTIFIER
L-Glutathione reduced	Sigma-Aldrich	Cat#G4251
MitoParaquat	Abcam	Cat#ab146819
Spautin-1	Sigma-Aldrich	Cat#SML0440
Tri-sodium Citrate dihydrate	Sigma-Aldrich	Cat#S4641
C13-GlutamineL-Glutamine (13C5,15N2)	Cambridge Isotope Laboratories	Cat#CNLM-1275-H-PK
L-[3,4-3H(N)]-Glutamine	Perkin Elmer	Cat#NET551250UC
Oligomycin	Sigma-Aldrich	Cat#O4876
FCCP	Sigma-Aldrich	Cat#C2920
Rotenone	Sigma-Aldrich	Cat#R8875
Antimycin A	Sigma-Aldrich	Cat#A8674
DMSO	Sigma-Aldrich	Cat#D2650
Human recombinant IL-3	R&D Systems	Cat#203-IL-010
Human recombinant IL-6	R&D Systems	Cat#206-IL-010
rhuSCF	Amgen	N/A
Stem Spam CC100	Stem Cell	Cat#02690
EPREX	Janssen	Cat#3400936992368
Human holo-transferrin	Sigma-Aldrich	Cat#T0665
Human insulin solution	Sigma-Aldrich	Cat#9278
Heparin	Sanofi	Cat#3400930484500
Bovine serum albumin	Sigma-Aldrich	Cat#A8806
IMDM	Life Technologies/ThermoFisher	Cat#21980032
StemSpam SFEM	Stem Cell	Cat#09650
StemSpam H3000	Stem Cell	Cat#09850
RPMI w/o glutamine and glucose	Pan Biotech	Cat#P04-17550
Seahorse XF Assay Medium	Agilent Technologies	102365-100
Seahorse XF Calibrant Solution	Agilent Technologies	100840-000
Ultima Gold liquid scintillation cocktail	Perkin Elmer	Cat#6013329
Critical commercial assays		
Anti-hCD34 MicroBead kit	Miltenyi Biotec	Cat#130-046-702; RRID:AB_2848167
RNeasy Mini kit	QIAGEN	Cat# 74104
QuantiTect™ Reverse Transcription Kit	QIAGEN	Cat# 205311
Experimental models: cell lines		
Jurkat E6-1	ATCC	TIB-152
293 T cells	ATCC	CRL-3216
Oligonucleotides		
IDH1 forward: 5′- GGGTTGGCCTTTGTATCTGA-3′	IDT	Custom order
IDH1 reverse: 5′- TTTACAGGCCCAGATGAAGC-3′	IDT	Custom order
IDH2 forward: 5′- TGGCTCAGGTCCTCAAGTCT-3′	IDT	Custom order
IDH2 reverse: 5′- CTCAGCCTCAATCGTCTTCC-3′	IDT	Custom order

REAGENT or RESOURCE	SOURCE	IDENTIFIER
IDH3a forward: 5′- GCGCAAAACATTTGACCTTT-3′	IDT	Custom order
IDH3a reverse: 5′- TGCACGACTCCATCAACAAT-3′	IDT	Custom order
TET2 forward: 5′- AGCAGCAGCCAATAGGACAT-3′	IDT	Custom order
TET2 reverse: 5′- AGGTTCTGTCTGGCAAATGG-3′	IDT	Custom order
bactin forward: 5′- GTCTTCCCCTCCATCGTG-3′	IDT	Custom order
bactin reverse: 5′- TTCTCCATGTCGTCCCAG-3′	IDT	Custom order
Recombinant DNA		
TRC2pLKO sh Tet2	Sigma Aldrich	Cat# TRCN0000418976
TRC2pLKO sh IDH1	Sigma Aldrich	Cat# TRCN0000312463
TRC1pLKO sh IDH1	Sigma Aldrich	Cat# TRCN0000027284
TRC1pLKO sh non-mammalian control	Sigma Aldrich	Cat# SHC002
Software and algorithms		
FlowJo (version 10)	BD Biosciences	https://www.flowjo.com/
Prism (version 8)	GraphPad Software	https://www.graphpad.com/scientific-software/prism/
Wave (version 2)	Agilent Technologies	https://www.agilent.com/en/product/cell-analysis/real-time-cell-metabolic-analysis/xf-software/seahorse-wave-desktop-software-740897
Xcalibur 2.2	ThermoFisher	http://www.casco-documentation.com/content/dam/tfs/ATG/CMD/cmd-documents/oper/oper/ms/lc-ms/soft/Man-XCALI-97209-Xcalibur-22-Acquisition-ManXCALI97209-D-EN.pdf
LCquan 2.7	ThermoFisher	https://assets.thermofisher.com/TFS-Assets/CMD/manuals/LCquan-Admin-2-7.pdf
TraceFinder 4.1	ThermoFisher	https://www.thermofisher.com/us/en/home/industrial/mass-spectrometry/liquid-chromatography-mass-spectrometry-lc-ms/lc-ms-software/lc-ms-data-acquisition-software/tracefinder-software.html
Other		
CM-H2DCFDA	Molecular Probes/Thermofisher	Cat#C6827
Dihydrorhodamine 123	Molecular Probes/Thermofisher	Cat#D23806
Mitotracker Deep Red FM	Molecular Probes/Thermofisher	Cat#M22426
MitoTracker Green FM	Molecular Probes/Thermofisher	Cat#M7514
MitoTracker Red CMXRos	Molecular Probes/Thermofisher	Cat#M7512
MitoSox Red	Molecular Probes/Thermofisher	Cat#M36008
Propidium Iodide	Sigma-Aldrich	Cat#P4170
Syto16	Molecular Probes/Thermofisher	Cat#S7578
Syto60	Molecular Probes/Thermofisher	Cat#S11342